GEOLOGIC MODELING AND SIMULATION REPORT FOR THE AQUISTORE PROJECT

Plains CO_2 Reduction (PCOR) Partnership Phase III
Task 1 – Deliverable D93

Prepared for:

Andrea M. Dunn

National Energy Technology Laboratory
U.S. Department of Energy
626 Cochrans Mill Road
PO Box 10940
Pittsburgh, PA 15236-0940

DOE Cooperative Agreement No. DE-FC26-05NT42592

Prepared by:

Wesley D. Peck
Robert C.L. Klenner
Guoxiang Liu
Charles D. Gorecki
Edward N. Steadman

Energy & Environmental Research Center
University of North Dakota
15 North 23rd Street, Stop 9018
Grand Forks, ND 58202-9018

March 2014
2014-EERC-07-09 Approved

EERC DISCLAIMER

LEGAL NOTICE This research report was prepared by the Energy & Environmental Research Center (EERC), an agency of the University of North Dakota, as an account of work sponsored by the U.S. Department of Energy (DOE) National Energy Technology Laboratory (NETL). Because of the research nature of the work performed, neither the EERC nor any of its employees makes any warranty, express or implied, or assumes any legal liability or responsibility for the accuracy, completeness, or usefulness of any information, apparatus, product, or process disclosed or represents that its use would not infringe privately owned rights. Reference herein to any specific commercial product, process, or service by trade name, trademark, manufacturer, or otherwise does not necessarily constitute or imply its endorsement or recommendation by the EERC.

ACKNOWLEDGMENT

This material is based upon work supported by DOE NETL under Award No. DE-FC26-05NT42592.

DOE DISCLAIMER

This report was prepared as an account of work sponsored by an agency of the United States Government. Neither the United States Government, nor any agency thereof, nor any of their employees, makes any warranty, express or implied, or assumes any legal liability or responsibility for the accuracy, completeness, or usefulness of any information, apparatus, product, or process disclosed, or represents that its use would not infringe privately owned rights. Reference herein to any specific commercial product, process, or service by trade name, trademark, manufacturer, or otherwise does not necessarily constitute or imply its endorsement, recommendation, or favoring by the United States Government or any agency thereof. The views and opinions of authors expressed herein do not necessarily state or reflect those of the United States Government or any agency thereof.

NDIC DISCLAIMER

This report was prepared by the EERC pursuant to an agreement partially funded by the Industrial Commission of North Dakota, and neither the EERC nor any of its subcontractors nor the North Dakota Industrial Commission (NDIC) nor any person acting on behalf of either:

(A) Makes any warranty or representation, express or implied, with respect to the accuracy, completeness, or usefulness of the information contained in this report or that the use of any information, apparatus, method, or process disclosed in this report may not infringe privately owned rights; or

(B) Assumes any liabilities with respect to the use of, or for damages resulting from the use of, any information, apparatus, method, or process disclosed in this report.

TABLE OF CONTENTS

LIST OF FIGURES iii

LIST OF TABLES iv

EXECUTIVE SUMMARY v

INTRODUCTION 1

APPROACH 1

PETROPHYSICAL ANALYSIS 4

STRUCTURAL ANALYSIS 4

DATA ANALYSIS 6

PETROPHYSICAL MODELING 10
- Porosity and Vshale 10
- Permeability 11
- Temperature and Pressure 12
- Water Saturation and Salinity 13
- Uncertainty Analysis and Optimization 13

MODEL REFINEMENT 13

UPSCALING AND GRID REFINEMENT 14

STATIC STORAGE ASSESSMENT 15

DYNAMIC SIMULATION 17

MODEL SETTINGS 17

NUMERICAL TUNING 18

SIMULATION RESULTS AND DISCUSSION 20
- 50-year Injection Period 20
- 5-year and 1-year Injection Periods 22
  - High Injection Rate vs. Low Injection Rate 22
- 5-year Injection Period vs. 1-year Injection Period 22
- Relative Permeability Sensitivity 24

Continued…

TABLE OF CONTENTS (continued)

CO_2 Breakthrough to the Observation Well 24
Pressure Differences 27

CONCLUSIONS AND FUTURE WORK 27

ACKNOWLEDGMENTS 29

REFERENCES 29

SIMULATION RESULTS OF CO_2 MOVEMENT AND PRESSURE DIFFERENCE OVER TIME ..... Appendix A

LIST OF FIGURES

1 Regional model that includes portions of North Dakota and Saskatchewan, with an area of 3670 mi^2, and a refined model of 13.1 mi^2 around the observation and injection wells 2

2 Workflow for the Aquistore model, which includes log analysis, structural correlation and analysis, data analysis, petrophysical modeling, uncertainty and optimization, and model refinement and upscaling 3

3 Petrophysical results of the Aquistore injection well displayed with routine core analysis porosity data for sidewall (red) and whole (black) core 5

4 Structural top of the basal aquifer and location of the PTRC injection well 6

5 N–S (A–A') and W–E (B–B') cross-sectional lines 7

6 Cross-sectional and well log displays of the Vshale and total porosity, respectively, and corresponding sand/shale zones 8

7 Isopach of the basal aquifer (top of Black Island to top of Precambrian) and location of the PTRC injection well 9

8 Porosity and permeability crossplot used as a direct input to honor the bivariate relationship between the two variables 11

9 Distributed total porosity near the Aquistore injection well 12

10 Distributed Vshale property near the Aquistore injection well 12

11 Structural top of the basal aquifer acquired from the 3-D seismic survey, showing increased resolution and structural features 14

12 Local grid refinement created to keep the grid resolution around the observation and injection wells while reducing the overall model cell size to increase and optimize the dynamic simulation 16

13 Relative permeability curves for the two samples 18

14 Relative permeability curves used for the simulation 19

15 Relative permeability fitted for the CMG simulation based on data tested by the EERC Applied Geology Laboratory 20

Continued…

LIST OF FIGURES (continued)

16 Total injected CO_2 and real injection rate for Cases 1–3 21

17 Total injected CO_2 by mass for Cases 1 and 2 22

18 Total injected CO_2 and injection rate for Cases 4 and 5 23

19 Total injected CO_2 and injection rate for Cases 6–9 23

20 Total injected CO_2 by mass for Cases 4–9 24

21 Cross-sectional view of CO_2 breakthrough in Cases 4 and 5 with high injection rate 25

22 Cross-sectional view of CO_2 breakthrough in Cases 6 and 8 with low injection rate..... 26

23 Cross-sectional view of CO_2 breakthrough in Cases 7 and 9 with low injection rate utilizing the relative permeability tested by the EERC Applied Geology Laboratory..... 28

LIST OF TABLES

1 Thickness Values for the Individual Reservoir and Nonreservoir Zones 9

2 Major and Minor Horizontal and Vertical Variogram Ranges for the Calculated Properties from the Petrophysical Analysis 10

3 Major and Minor Horizontal and Vertical Variogram Ranges for Upscaled Logs from Pseudowells 15

4 CO_2 Storage Potential for the Black Island and Deadwood Formations in the Area Around the Aquistore Project..... 17

5 Results Summary for Nine Cases by Varying Simulation Factors 21

GEOLOGIC MODELING AND SIMULATION REPORT FOR THE AQUISTORE PROJECT

EXECUTIVE SUMMARY

The Plains CO_2 Reduction (PCOR) Partnership, through the Energy & Environmental Research Center (EERC), in collaboration with the Petroleum Technology Research Centre (PTRC), has constructed static and dynamic geologic models to simulate and assess the potential carbon dioxide (CO_2) storage at the Aquistore site. The Aquistore project is part of the world's first commercial postcombustion carbon capture, utilization, and storage project from a coal-fired power-generating facility, the SaskPower Boundary Dam, located in Saskatchewan, Canada, and will be acting as a storage site for a portion of the captured CO_2 from the Boundary Dam power plant. The Aquistore site includes one injection well and a 500-foot offset observation well. Both wells were drilled and completed in the Deadwood and Black Island Formations. At the time of this report, injection at the Aquistore site is anticipated to begin in mid- to late 2014.

To better understand the storage implications of injecting at the Aquistore site, the EERC developed a geocellular model of the basal saline system for the dual purposes of determining the static CO_2 storage capacity and as a basis to run detailed reservoir simulation to determine injectivity, dynamic storage capacity, and breakthrough time at the observation well. To compensate for a lack of well control locally, a regional-scale model was first constructed to determine the regional stratigraphic reservoir and nonreservoir zones. From this regional model, a fine-scale model was confined to the extent of the 13.1-square-mile PTRC 3-D seismic survey area, with higher structural resolution. Integration of the data derived from the regional model and the data from the 3-D seismic survey helped create a robust and heterogeneous model around the Aquistore injection well and the observation well.

As a first pass, the detailed 13.1-square-mile model was used to estimate a static storage capacity employing the U.S. Department of Energy methodology and resulted in a range of static storage resource of approximately 8.4 to 27.1 Mt for the P10 to P90 confidence intervals, respectively. This result indicated that our model was probably big enough to model a short- to medium-duration injection of perhaps 5–30 years at 1 Mt/yr; however, it may be too small to adequately simulate a 50-year injection period.

To further evaluate the targeted saline system, and thus its viability as a potential storage horizon for CO_2, the geocellular model was used as the framework for an assessment of the dynamic storage capacity of the system. Two scenarios were designed based on the static geologic model. The first investigated the injectivity of the system and the timing of CO_2

breakthrough at the observation well in a 13.1-mi^2 area. The second scenario, which will be detailed in a subsequent report, encompasses a 3670-mi^2 area. As part of this investigation, core plug analysis and relative permeability studies were also conducted on samples provided from the injection well core. Information from these analyses was integrated into the construction of the geocelluar model and the dynamic simulations and will be provided in a subsequent report.

A total of nine simulation cases were run to investigate factors such as boundary conditions, injection rates, and time length. The injection duration for these scenarios was set at 1, 5, and 50 years, and the injection rates were set at 1 Mt/yr and 0.3 Mt/yr. Although the maximum injection rate in the model was set as 1 Mt/yr, the maximum attained in the model was 0.73 Mt/yr because of bottomhole pressure limitations. The total mass of CO_2 injected in the 50-year cases ranged from 1.5 to 33.6 Mt, with the large range in values a result of changing the boundary conditions from closed to open. CO_2 storage values for the 5-year cases range from 1.5 to 3.6 Mt, and those for the 1-year cases range from 0.3 to 0.7 Mt.

An important aspect of this investigation with regard to potential monitoring efforts is the timing of CO_2 breakthrough at the observation well. The earliest breakthrough occurred between 10 and 15 days at the higher injection rate (0.73 Mt/yr), and the projected CO_2 path follows the top reservoir zone of the Deadwood Formation. At the lower injection rate (0.3 Mt/yr), breakthrough happens between 25 and 30 days after injection and follows the same path. Overall, CO_2 breakthrough in most of the reservoir zones happens in about 3 months for the low injection rate; this time is reduced to 45 days at the higher rate. Based on the information derived from the various simulation cases, the CO_2 breakthrough will most likely happen in the first month of injection regardless of the injection rate and assumptions of relative permeability.

Based on the simulation results, the storage of CO_2 in the study area using the existing two-well configuration is feasible, depending on the volume of CO_2 that need to be injected and stored from the neighboring Boundary Dam power plant. Generally, the maximum injectivity for the current injection well could reach 0.73 Mt/yr based on the geological characterization of the study area. However, this could be improved through optimization operations such as adding additional injection wells, utilizing formation water extraction wells, and/or the use of horizontal injection wells. All of these additional optimization techniques will be investigated in the next phase of work and reported on in a subsequent report. In addition, the larger regional-size model will be utilized to provide better insights with respect to a commercial-scale injection rate over a long period of time. Finally, future work will also include geomechanical, geochemical, and geothermal behaviors and integrate them throughout the entire modeling and simulation process to investigate the role these variables may play in CO_2 storage at the Aquistore site.

GEOLOGIC MODELING AND SIMULATION REPORT FOR THE AQUISTORE PROJECT

INTRODUCTION

The Plains CO_2 Reduction (PCOR) Partnership, through the Energy & Environmental Research Center (EERC), is collaborating with the Petroleum Technology Research Centre (PTRC) on site characterization; modeling and simulation; risk assessment; public outreach; and monitoring, verification, and accounting (MVA) activities for the Aquistore project. The Aquistore project is a carbon capture, utilization, and storage (CCUS) project situated near the town of Estevan, Saskatchewan, Canada, and the U.S.–Canada border. This project is managed by PTRC and will serve as buffer storage of carbon dioxide (CO_2) from the SaskPower Boundary Dam CCUS project, the world's first commercial-scale postcombustion CCUS project from a coal-fired electric generating facility. To date, an injection well and an observation research well (~500 ft apart) have been drilled and completed at the Aquistore site, with injection anticipated to begin in 2014. Using a combination of site characterization data provided by PTRC and independently acquired information, the PCOR Partnership has constructed a static geologic model to assess the potential storage capacity of the Aquistore site and provide the foundation for dynamic simulation. The geologic model and the results of the predictive simulations will be used in the risk assessment process to help define an overall monitoring plan for the project and to assure stakeholders that the injected CO_2 will remain safely stored at the Aquistore site.

The deep saline system targeted for storage comprises the Deadwood and Black Island Formations, the deepest sedimentary units in the Williston Basin. At nearly 11,500 ft below the surface, this saline system is situated below most oil production and potash-bearing formations in the region and provides a secure location for the storage of CO_2. Characterization data acquired from the Aquistore site for these formations include a 3-D seismic survey, petrophysical core data, and a comprehensive logging suite.

APPROACH

A geocellular model of the basal saline system was built and centered on the Aquistore injection well and observation well to determine static CO_2 storage volumes. This model is also used in the dynamic simulation scenarios to determine CO_2 movement, reservoir response, and dynamic storage. A regional-scale model was initially built with an approximate area of 3670 mi^2. The model was then clipped and optimized to the same extent as the 13.1 mi^2 3-D seismic survey conducted by PTRC (Figure 1).

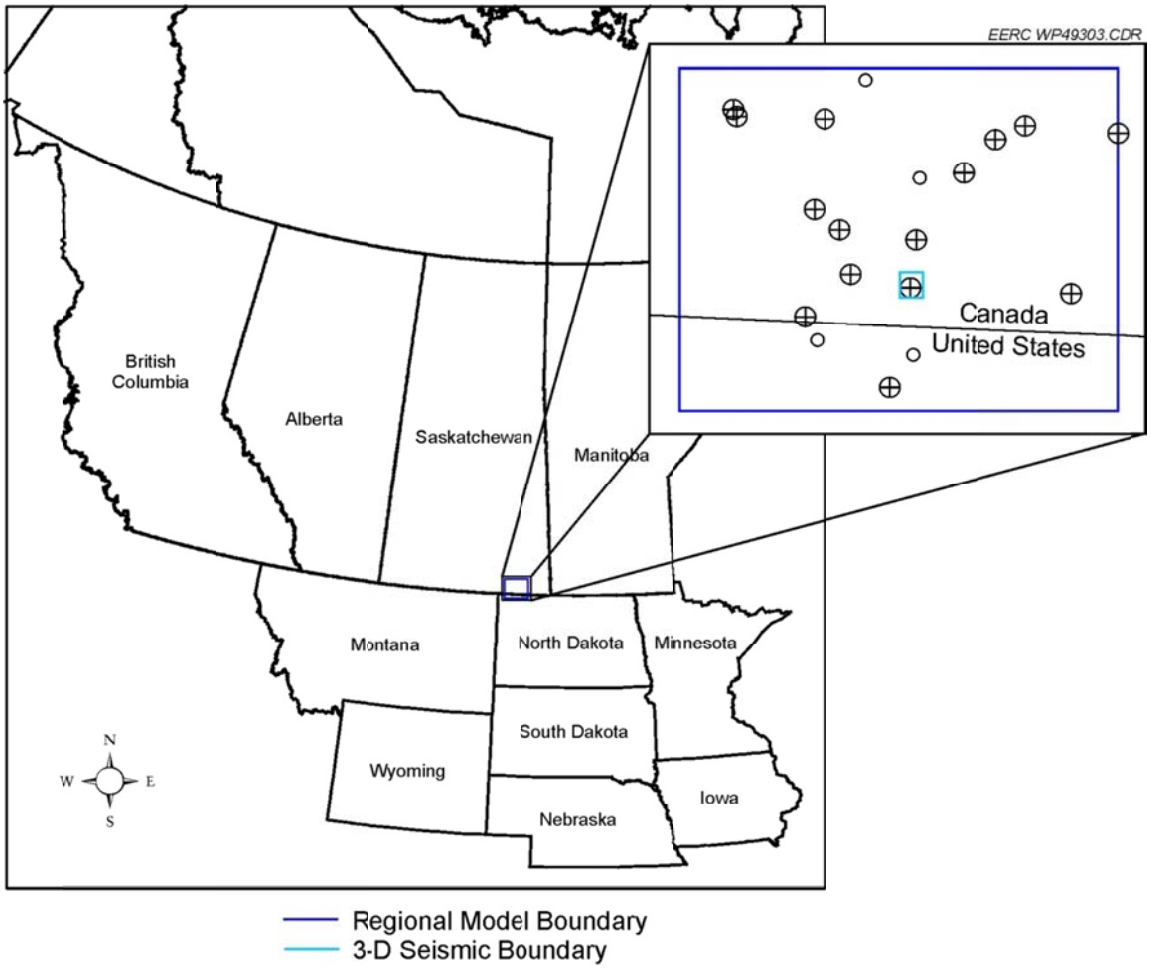

Figure 1. Regional model that includes portions of North Dakota and Saskatchewan, with an area of 3670 mi^2, and a refined model of 13.1 mi^2 around the observation and injection wells.

The lack of wells within the vicinity of the Aquistore injection well and observation well prompted the production of a larger-scale, regional model. The lack of well control poses problems when distributing the petrophysical properties without any knowledge of variogram ranges or stratigraphic continuity of good or poor geologic zones. The regional model determined how the reservoir correlated laterally in the aquifer, while the 3-D seismic survey provided a higher structural resolution for the storage unit, including the Icebox, Black Island, Deadwood, and Precambrian Formations. Integration of the data derived from the regional model and the data from the 3-D seismic survey helped create a robust and heterogeneous model around the Aquistore wells.

The workflow for model development and optimization included petrophysical log analysis, stratigraphic correlation, structural analysis, data analysis, petrophysical modeling, uncertainty analysis, and upscaling (Figure 2). The petrophysical log analysis was performed on 15 wells to derive shale volumes and total porosity using available wireline log data. The results were also calibrated to data measured from routine core analysis data performed on whole and sidewall core. The shale volume derived by the petrophysical analysis was used to divide the

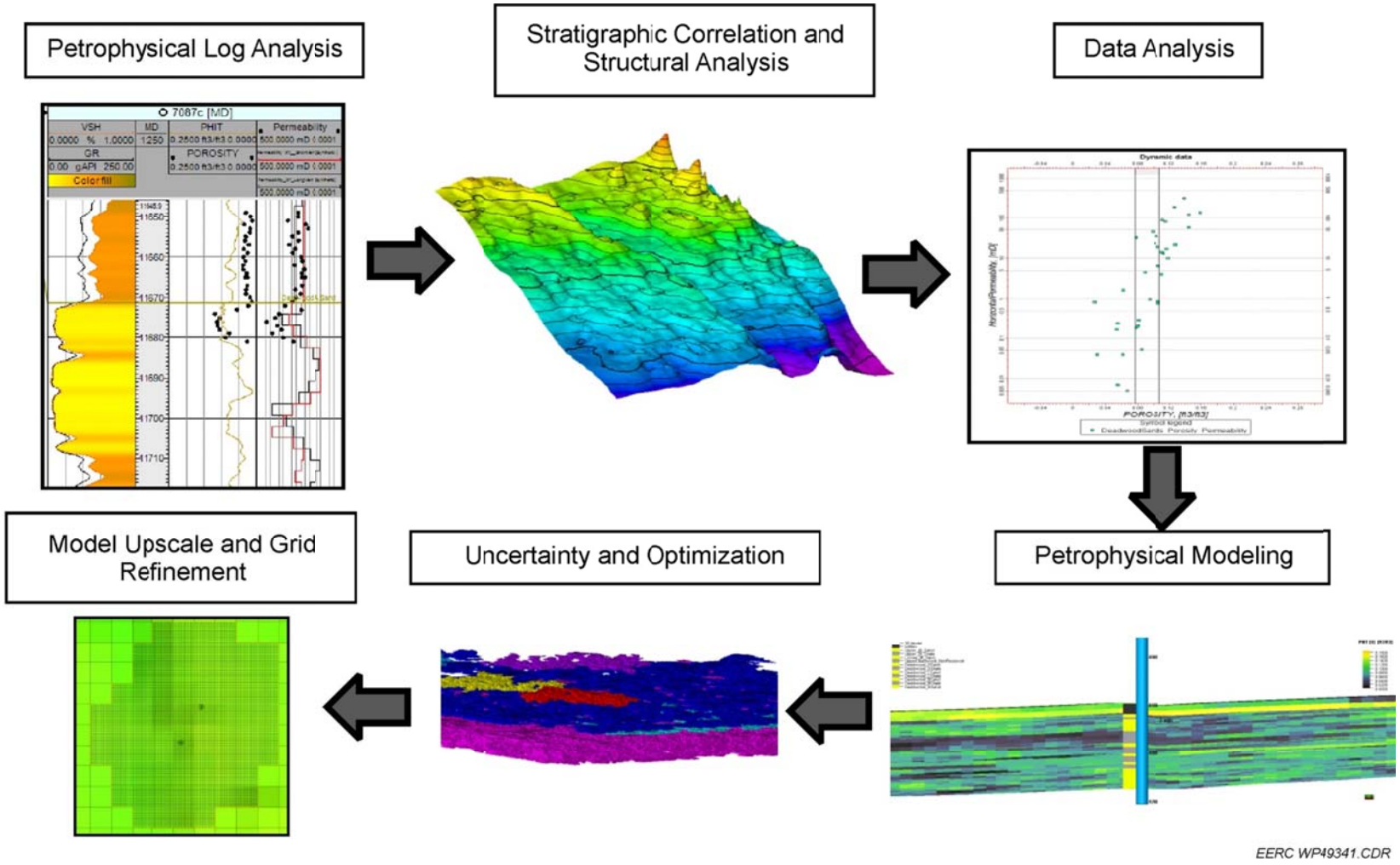

Figure 2. Workflow for the Aquistore model, which includes log analysis, structural correlation and analysis, data analysis, petrophysical modeling, uncertainty and optimization, and model refinement and upscaling.

model into 12 traceable zones, including six sand units and six shale units throughout the regional study area. Total porosity and shale volume was then stochastically populated throughout the model, with each zone using the upscaled logs and variogram ranges determined through data analysis. Effective porosity was then calculated for each cell, and permeability was populated based on its empirical relationship with porosity. The model was populated with additional reservoir properties including pressure and temperature, which are important in calculating CO_2 density at reservoir conditions and for inputs into the dynamic simulation model. After an uncertainty analysis was performed, the model was clipped to the area of the 3-D seismic survey, where structural resolution is higher, and the workflow was applied again for further optimization.

PETROPHYSICAL ANALYSIS

Petrophysical analysis on well logs was performed using Schlumberger's Techlog on 15 wells. These wells include the Aquistore observation and injection wells, three wells in North Dakota, and ten wells in Saskatchewan. The workflow for the petrophysical analysis included log quality control, gamma ray normalization, calculation of both Vshale and total porosity, and a quality check of the results in comparison to the core results.

Total porosity and Vshale were calculated for the 15 wells using the neutron density and gamma ray methods, respectively. Porosity results were quality-checked and calibrated using routine core analysis data from sidewall and whole core (Figure 3). Vshale was calculated using the normalized gamma ray logs and readings of 215 and 10 for the shale and matrix, respectively. The calculation underwent a Monte Carlo analysis to determine uncertainty in these values, which resulted in a mean value for Vshale from the 100 iterations.

These Vshale results were useful in subdividing the reservoir into sand and shale zones. Furthermore, effective porosity was calculated using results of the Vshale and total porosity (Eq. 1). A porosity of 14% was determined for shale and was further investigated by performing an uncertainty analysis on the values and its overall effect on the net-to-gross calculations.

$$PHIe = PHIT - (PHIT_{shale} * V_{shale}) \quad \text{[Eq. 1]}$$

Where PHIT is the total porosity, PHIE is the effective porosity, V_{shale} is the volume of shale, and $PHIT_{shale}$ is the porosity of the 100% shale matrix.

STRUCTURAL ANALYSIS

The reservoir portion of the model, which is the planned target for CO_2 storage, comprises the Black Island and Deadwood Formations. These formations consist of alternating layers of sand and shale or reservoir and nonreservoir rock. The structural top of the model is the Icebox shale, which serves as the top reservoir seal; the structural base of the model is the Precambrian basement rock consisting of igneous or metamorphosed rock. As shown in Figure 4, the overall structure in the model follows the general structure of the Williston Basin. Any faulting or folding structural features that may be present in the regional model are not recognized because of the lack of control points.

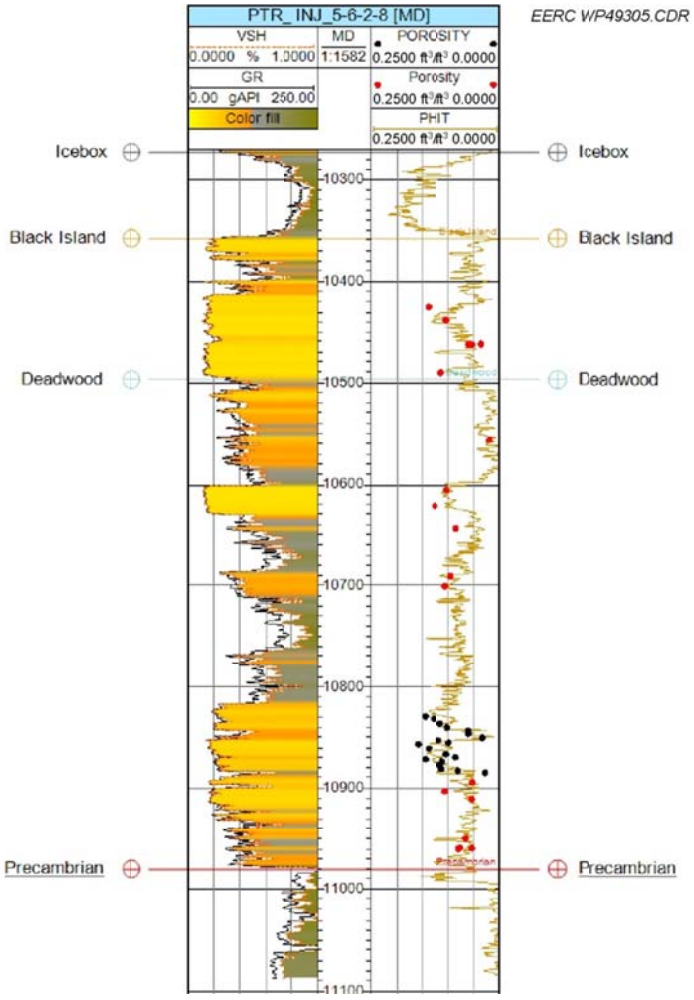

Figure 3. Petrophysical results of the Aquistore injection well displayed with routine core analysis porosity data for sidewall (red) and whole (black) core.

To further characterize the reservoir formations, the Vshale log was used to stratigraphically correlate sand and shale sequences (Figures 5 and 6). The sand packages, with occasional silt and carbonate stringers, are the reservoir zones with high total porosity and low shale volumes. These zones are widespread and correlative units over the study area. Subdividing the reservoir system into these zones helps distribute the petrophysical properties accurately and better define the vertical and lateral heterogeneity of the model.

Structural and isochore surfaces were generated from the stratigraphic picks using a convergent interpolation algorithm within the Petrel software. These isochore surfaces helped eliminate structural surface crossover where well control was lacking. The total reservoir thickness varies from 112 to 653 feet over the study area (Figure 7). Thickness ranges for the Black Island and Deadwood Formations are 87–160 and 0–510 feet, respectively. Individual thicknesses for each sand and shale zone are displayed in Table 1.

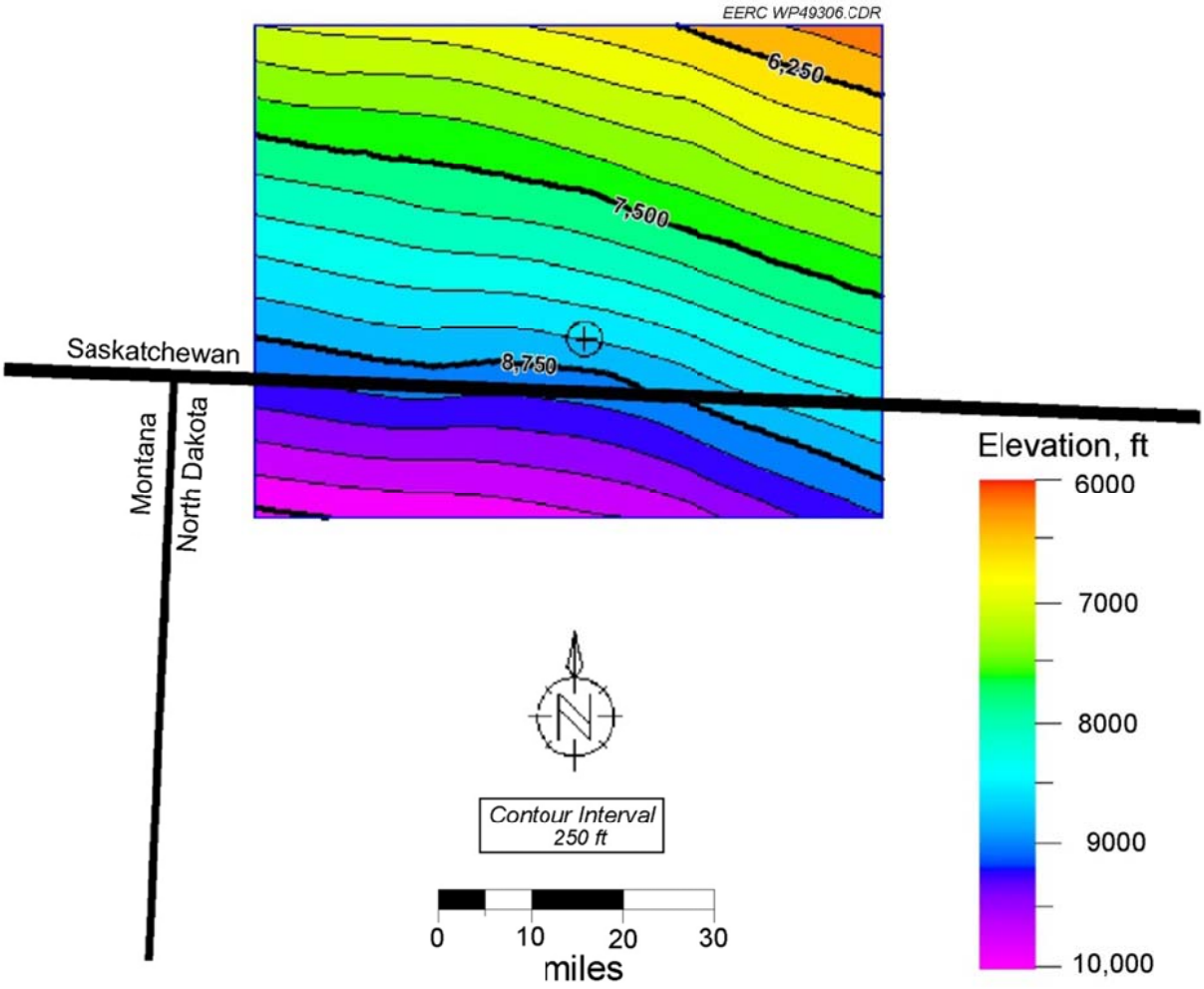

Figure 4. Structural top of the basal aquifer and location of the PTRC injection well.

DATA ANALYSIS

Prior to data analysis, the wells were upscaled accordingly by property and zone. The data analysis consists of a geostatistical investigation of the upscaled data by performing data transformations. These data transformations helped derive model variograms by detrending and normalizing the upscaled data for each zone and property. Variograms modeled in the vertical direction help optimize layering or cell height for each zone and the vertical distribution of properties. Variograms determined in the x and y directions help distribute the properties geospatially in the lateral directions.

Each zone is spatially different, and changes in the variogram from one zone to the next can be caused by changes in lithology, depositional environment, diagenesis, and much more. Table 2 presents the expanded-model exponential variogram ranges for the calculated properties from the petrophysical analysis.

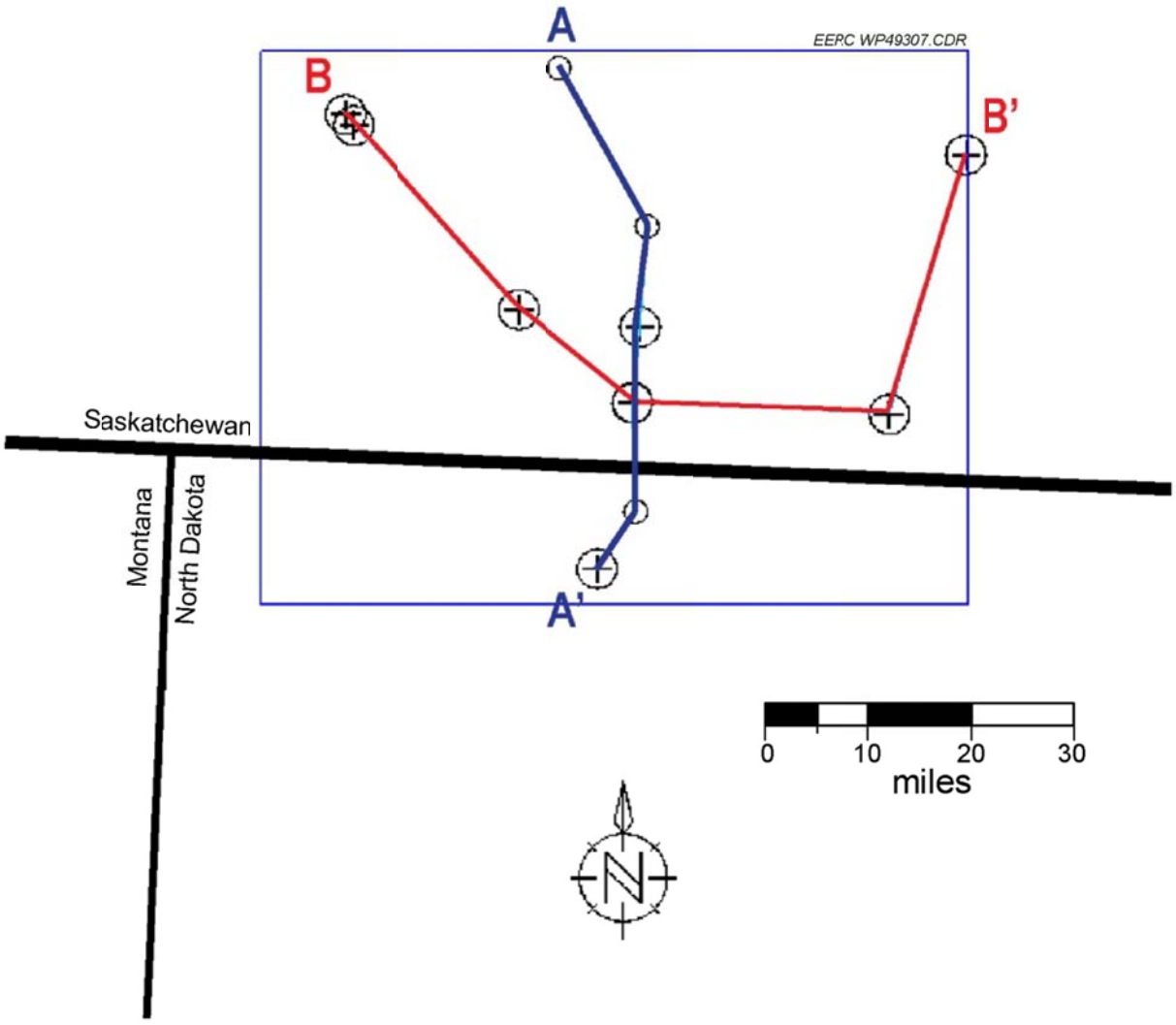

Figure 5. N–S (A–A') and W–E (B–B') cross-sectional lines (depicted in Figure 6).

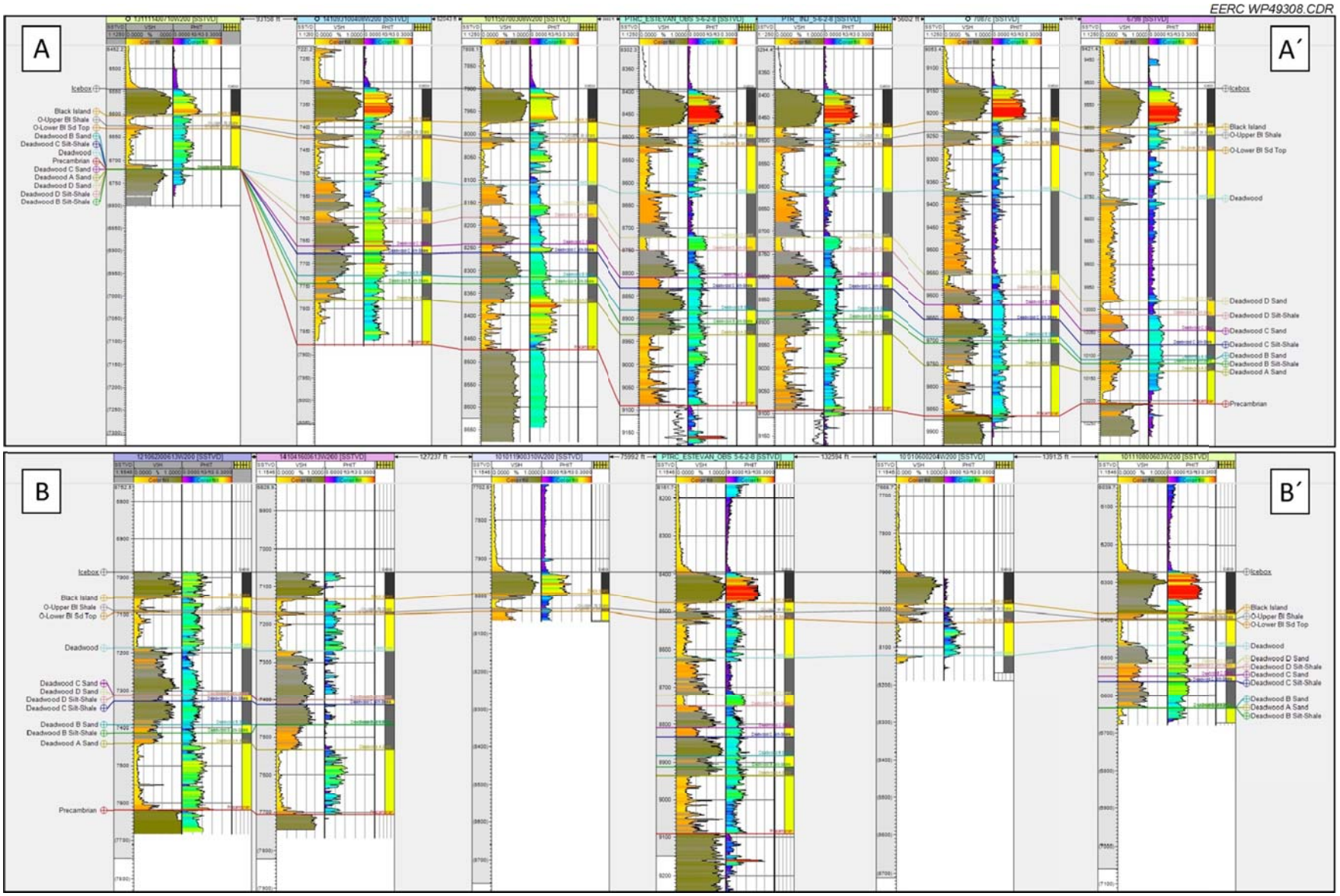

Figure 6. Cross-sectional and well log displays of the Vshale and total porosity, respectively, and corresponding sand/shale zones.

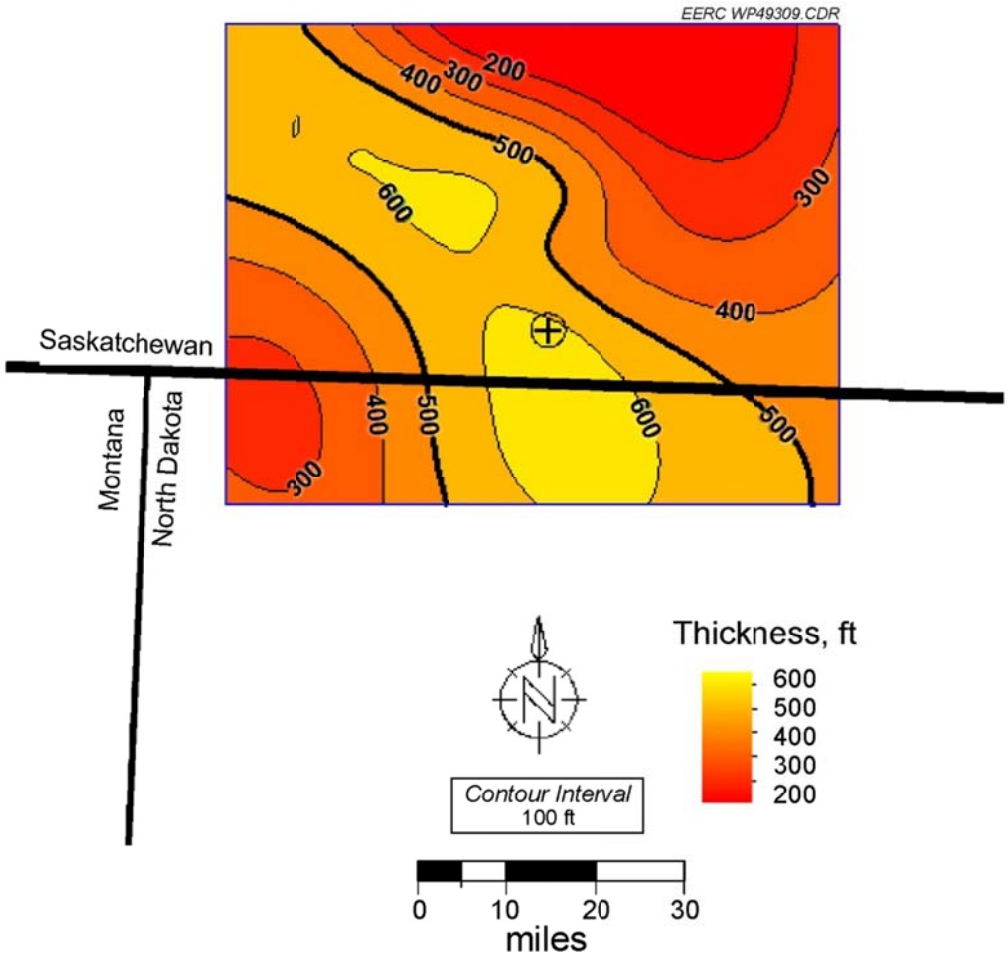

Figure 7. Isopach of the basal aquifer (top of Black Island to top of Precambrian) and location of the PTRC injection well.

Table 1. Thickness Values for the Individual Reservoir and Nonreservoir Zones, ft

Zone	Minimum	Maximum	Mean
Icebox Cap Rock	29	56	37
Upper Black Island Sand	1	8	5
Upper Black Island Shale	1	18	7
Lower Black Island Sand	3	5.5	5
Upper Deadwood Silt	0	82	27
Deadwood D Sand	0	5	3
Deadwood D Shale	0	35	15
Deadwood C Sand	0	5	2.5
Deadwood C Shale	0	36	19
Deadwood B Sand	0	5	1
Deadwood B Shale	0	41	19
Deadwood A Sand	0	5	2

Table 2. Major and Minor Horizontal and Vertical Variogram Ranges for the Calculated Properties from the Petrophysical Analysis (the vertical range had some uncertainty and was investigated during uncertainty analysis)

Zone	Upscaled Properties	Variogram Ranges, ft			
		Major	Minor	Short Vertical	Long Vertical
Icebox	Vshale and PHIT	36,000	36,000	37	75
Upper Black Island Sand	Vshale and PHIT	10,000	10,000	20	30
Upper Black Island Shale	Vshale and PHIT	15,000	15,000	7	20
Lower Black Island Sand	Vshale and PHIT	10,000	10,000	10	80
Upper Deadwood Nonreservoir	Vshale and PHIT	15,000	15,000	10	50
Deadwood D Sand	Vshale and PHIT	10,000	10,000	10	20
Deadwood D Shale	Vshale and PHIT	15,000	15,000	8	25
Deadwood C Sand	Vshale and PHIT	10,000	10,000	10	15
Deadwood C Shale	Vshale and PHIT	15,000	15,000	10	35
Deadwood B Sand	Vshale and PHIT	10,000	10,000	6	12
Deadwood B Shale	Vshale and PHIT	15,000	15,000	8	35
Deadwood A Sand	Vshale and PHIT	10,000	10,000	8	40

A bivariate analysis was also performed using the core porosity and permeability data. A crossplot of the data showed an empirical relationship between the Deadwood and Black Island sands (Figure 8). The resulting crossplots of the bivariate analysis are used as part of a cloud transform to populate permeability throughout the model based on the resulting stochastic porosity property.

PETROPHYSICAL MODELING

Porosity and Vshale

The petrophysical results and variograms, determined from data analysis, were used to populate the petrophysical properties using a stochastic Gaussian simulation. This simulation technique honors both the original histogram data and upscaled well logs, while utilizing the variogram to distribute the properties away from the wellbore. Quality assurance and quality control of the resulting property distribution were conducted using 3-D visualization and statistical review.

The distribution of total porosity and Vshale properties reveals the lateral and vertical heterogeneity throughout the reservoir (Figure 9 and 10). These resulting properties were then used to calculate an effective porosity based on a shale porosity of 14%, thus effectively removing that portion of porosity containing immovable clay-bound water for accurate fluid flow in the simulation. Calculating the effective porosity also is used to help accurately determine storage volumes and areas of interconnected reservoir during the optimization process.

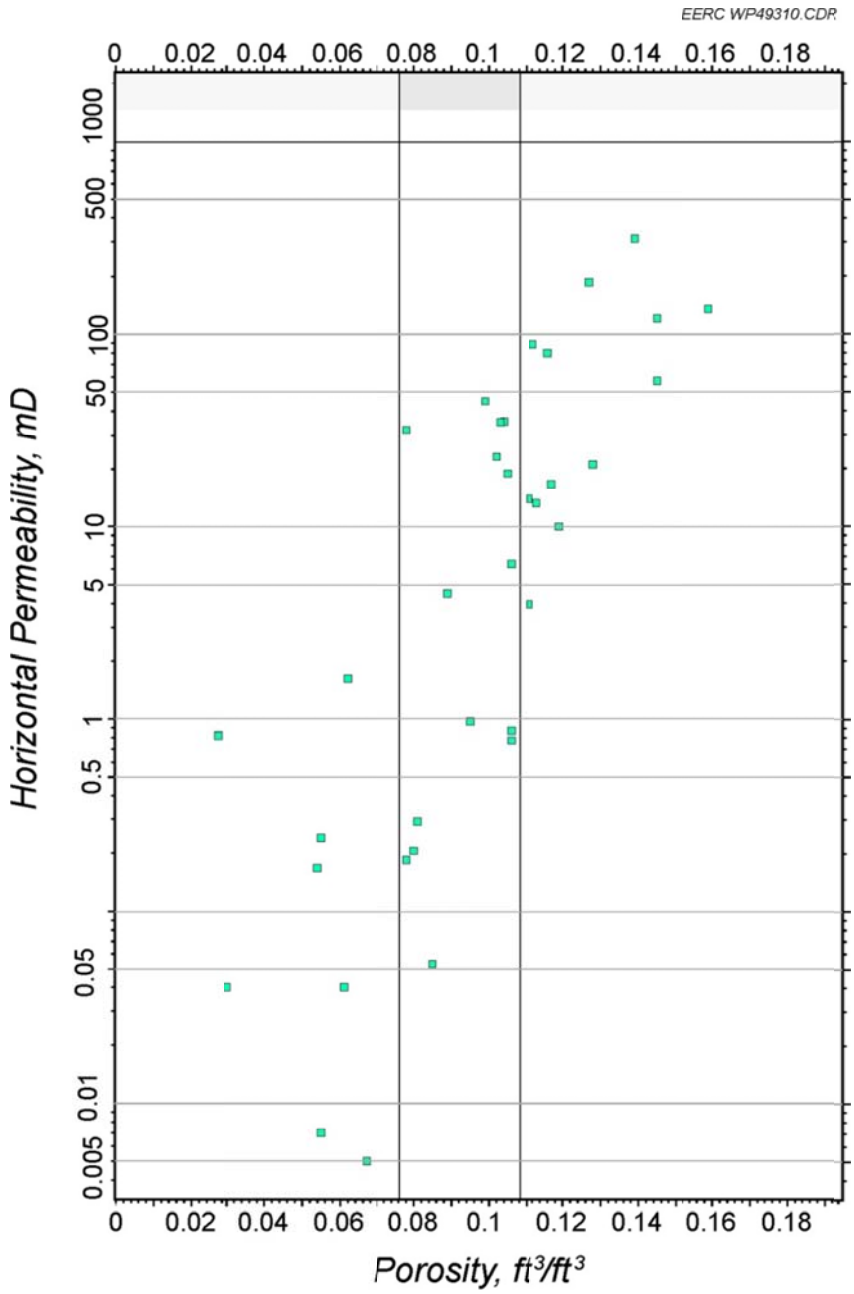

Figure 8. Porosity and permeability crossplot used as a direct input to honor the bivariate relationship between the two variables.

Permeability

Permeability in the model was distributed using the bivariate relationship determined from the porosity and permeability analysis from the core data. The crossplot is used as an input, and the relationship between porosity and permeability is honored. Furthermore, permeability for the shale zones shows no bivariate relationship and is more random, with permeability ranging from 0.09 to 0.9 mD.

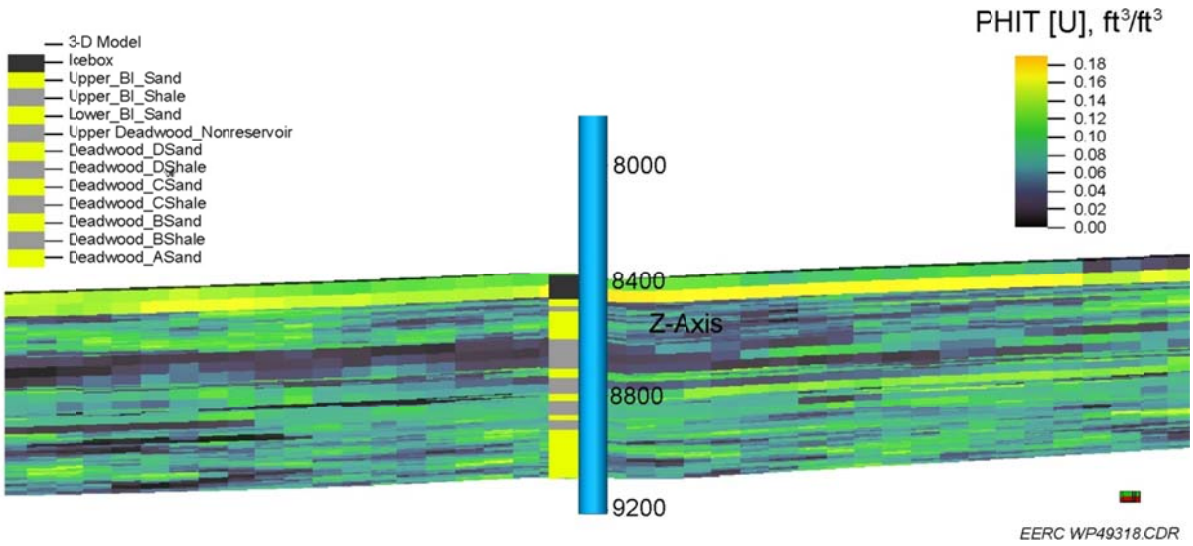

Figure 9. Distributed total porosity near the Aquistore injection well. A zonation log is displayed along the wellbore to show the reservoir (yellow) and nonreservoir zones (gray).

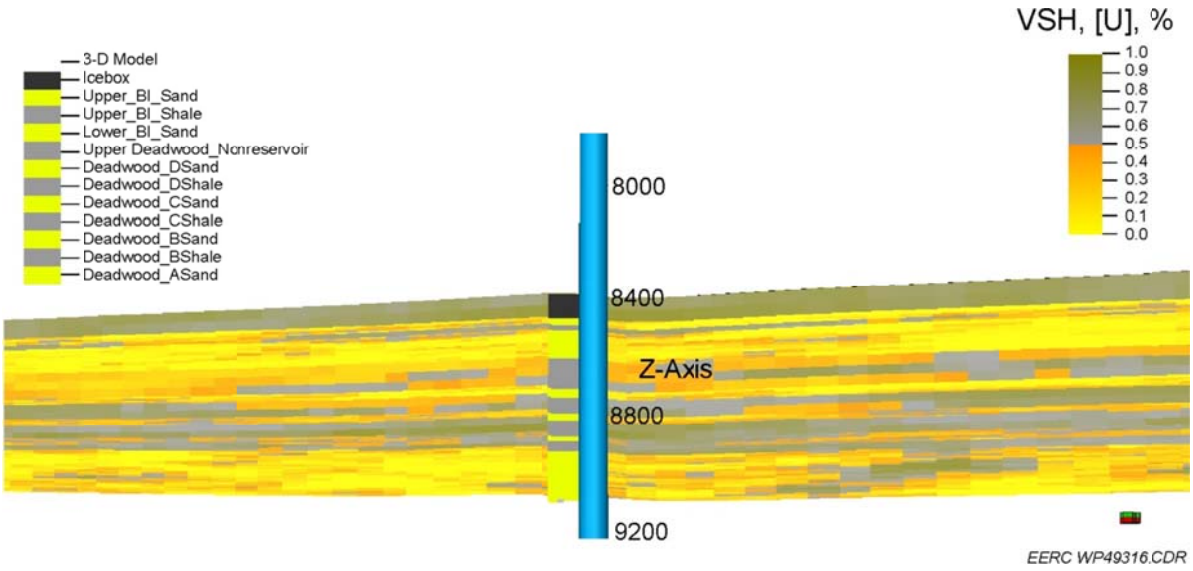

Figure 10. Distributed Vshale property near the Aquistore injection well. A zonation log is displayed along the wellbore to show the reservoir (yellow) and nonreservoir zones (gray).

Temperature and Pressure

CO_2 density is a function of both temperature and pressure. Modeling the pressure and temperature regime allows for CO_2 density to be modeled based on integrated changes to both properties throughout the saline system. Pressure determinations of the system are based on drillstem test (DST) measurements, while temperature was determined from corrected bottomhole temperature (BHT) and DST measurements. The measurements were contoured

using a kriging algorithm. The resulting contours show a lateral distribution of the properties but lack a vertical component. Vertical gradients of 0.47 psi/ft and 0.1°F/ft were used to populate the pressure and temperature properties vertically in the reservoir.

Water Saturation and Salinity

Because of the complexity of the aquifer spatially and the lack of well control in the model, a water saturation of 1 was populated throughout the model, resulting in the absence of oil and gas. Although oil and gas are known to present in the basal Cambrian formation, determining exactly how much and how they are distributed in the model is a challenge. However, water salinity in the model was calculated to determine salinity for the importance of CO_2 interactions with brine in the dynamic simulation. Salinity values were contoured from measurements and salinity determinations by Bachu and others (2011). Salinity values in the study area range from 271,000 to 336,000 ppm total dissolved solids.

Uncertainty Analysis and Optimization

An uncertainty analysis was performed to optimize the model and investigate the uncertainty in certain model-building parameters, including shale porosity, variogram range, structural interpolation, and net-to-gross reservoir. The results of the uncertainty analysis were then ranked accordingly by calculated pore volume, resulting in a low-, mid-, and high-volumetric case for the amount of pore volume accessible to store the potential injected CO_2. The selected midvolume case used data for model optimization within the area where the 3-D seismic survey was conducted.

MODEL REFINEMENT

The fine-scale model is confined to the extent of the 13.1 mi^2 3-D seismic survey area centered on the Aquistore observation well and injection well. The regional model was refined to a fieldwide model, with the increased structural resolution obtained from the 3-D seismic survey (Figure 11). The resolution of the fine-scale model was increased by decreasing the cell sizes from 1000 × 1000 ft to 25 × 25 ft. The layering, or vertical resolution, remained the same as in the regional scale model.

The interpreted 3-D seismic survey provided by PTRC identified stratigraphic tops throughout the study area for the Icebox, Black Island, Deadwood Formations, and the Precambrian surface. The development of the regional-scale model identified 12 distinct reservoir and nonreservoir zones present over the region, but these zones are not interpreted in the seismic survey. To help capture these zones stratigraphically, the data generated from the regional-scale model were integrated into the fine-scale model by creating four pseudowells. These wells were placed at the corners of the fine-scale model and given synthetic logs and log tops determined from the regional-scale model properties. The stratigraphic tops were then used to determine the reservoir and nonreservoir (sand/shale) zones away from the injection and observation wells and to capture the vertical heterogeneity in the study area.

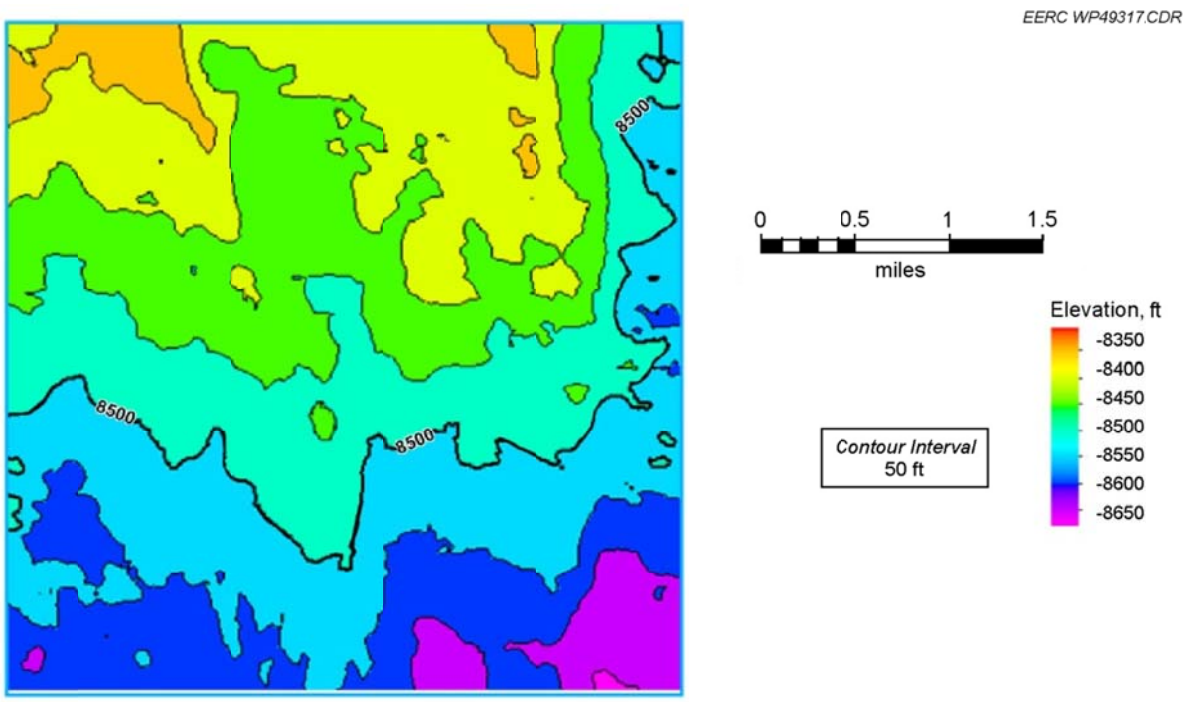

Figure 11. Structural top of the basal aquifer acquired from the 3-D seismic survey, showing increased resolution and structural features.

The model construction for the fine-scale model then included the same workflow steps as performed in the regional characterization effort. This included structural interpretation for the sand/shale zones, data analysis, petrophysical modeling, and upscaling. Data analysis was conducted again with an expanded-model to determine a field-scale exponential variogram range using the upscaled logs from the pseudowells and is presented in Table 3. Petrophysical properties were then distributed in the fine-scale model using the same methods as the regional-scale model.

After the distribution of petrophysical properties, an uncertainty analysis was performed once more on the variogram and net-to-gross calculations. The resulting pore volumes created a low-, mid-, and high-volumetric case. The resulting midvolume case was used for model upscaling and grid refinement for use in the dynamic simulation.

UPSCALING AND GRID REFINEMENT

The original fine-scale model was created using 25 × 25-ft cell blocks, resulting in a geologic model of 58 million cells. The resulting model would have required large amounts of computing time for simulation and would minimize the chances to run several injection scenarios based on the project time frame. In order to aid in the simulation process, the model was upscaled to reduce model size yet retain geologic heterogeneity.

Table 3. Major and Minor Horizontal and Vertical Variogram Ranges for Upscaled Logs from Pseudowells (the vertical range had some uncertainty and was investigated during the uncertainty analysis).

		Variogram Ranges, ft			
Zone	Upscaled Properties	Major	Minor	Short Vertical	Long Vertical
Icebox	Vshale and PHIT	5000	5000	40	80
Upper Black Island Sand	Vshale and PHIT	3000	3000	20	25
Upper Black Island Shale	Vshale and PHIT	5000	5000	10	18
Lower Black Island Sand	Vshale and PHIT	3000	3000	12	90
Upper Deadwood Nonreservoir	Vshale and PHIT	5000	5000	35	80
Deadwood D Sand	Vshale and PHIT	3000	3000	12	25
Deadwood D Shale	Vshale and PHIT	5000	5000	30	50
Deadwood C Sand	Vshale and PHIT	3000	3000	15	25
Deadwood C Shale	Vshale and PHIT	5000	5000	25	50
Deadwood B Sand	Vshale and PHIT	3000	3000	12	20
Deadwood B Shale	Vshale and PHIT	5000	5000	15	30
Deadwood A Sand	Vshale and PHIT	3000	3000	15	80

The upscaling process resulted in a model with 1.3 million cells by changing the lateral resolution and maintaining the vertical resolution. To maintain the geologic heterogeneity, local grid refinement (LGR) was used over an approximate radius of 10,000 ft around both the observation and injection well (Figure 12). The local grid refinement maintains the lateral and vertical heterogeneity by keeping the original 25 × 25-ft cell size. Outside of the LGR, the cell size was increased to 250 × 250 ft.

STATIC STORAGE ASSESSMENT

The methodology used in this study follows the approach described in DOE Atlas III (U.S. Department of Energy Office of Fossil Energy, 2010) which builds on the IEAGHG work of Gorecki and others (2009). It is based on the volumetric approach for estimating CO_2 storage resource potential saline formations. The volumetric equation to calculate the CO_2 storage resource mass estimate for geologic storage in saline formations is:

$$MCO_2e = A \times h \times \varphi \times \rho CO_2 \times E \qquad \text{[Eq. 2]}$$

The total area (A), gross formation thickness (h), and total porosity (φ) terms account for the total bulk volume of pore space available. The value for CO_2 density (ρ) converts the reservoir volume of CO_2 to mass. The storage efficiency factor (E) reflects the fraction of the total pore volume that will be occupied by the injected CO_2. For saline formations, the CO_2 storage efficiency factor is a function of geologic parameters, such as area, gross thickness, and total porosity, that reflect the percentage of volume amenable to CO_2 sequestration and displacement efficiency components that reflect different physical barriers inhibiting CO_2 from contacting 100% of the pore volume of a given basin or region. Volumetric methods are applied when it is generally assumed that the formation is open and that formation fluids are displaced

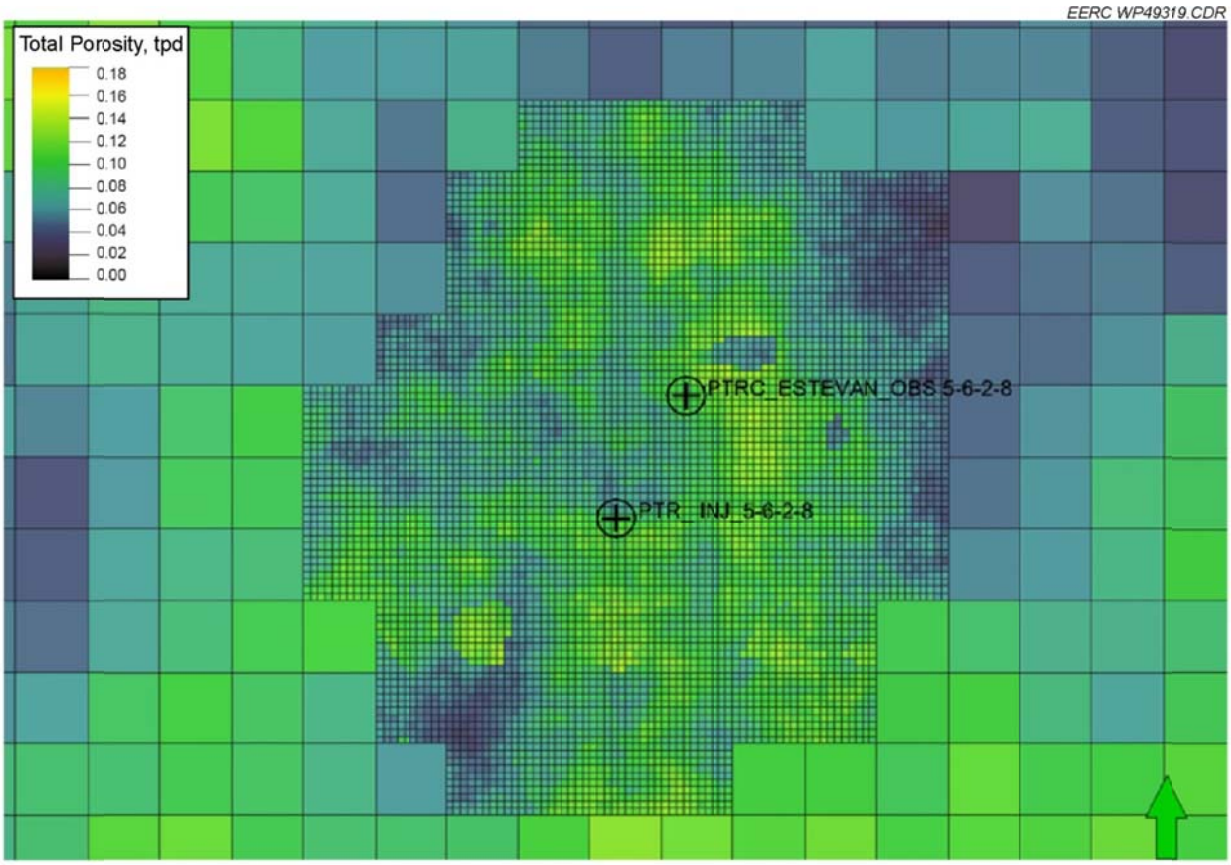

Figure 12. Local grid refinement created to keep the grid resolution around the observation and injection wells while reducing the overall model cell size to increase and optimize the dynamic simulation. Large cells are 250 × 250 ft and small cells are 25 × 25 ft.

from the formation or managed via production. The target system for the Aquistore Project is assumed to be an open system for the purpose of the static capacity calculation. A comprehensive discussion of the derivation of the methodology and the efficiency factor is presented in Gorecki and others (2009), U.S. Department of Energy Office of Fossil Energy (2010), and Goodman and others (2011).

The CO_2 density for the regional and local models was calculated based on the current reservoir pressure and temperature. CO_2 density at reservoir conditions is approximately 38 lb/ft^3. The resulting density was multiplied by the calculated pore volume and then multiplied by an efficiency factor to determine the mass of CO_2 that could be stored at reservoir conditions. The site-specific storage efficiency factor applied to the calculated mass is 14% at the P50 confidence level as established by Goodman and others (2011). This storage efficiency factor assumes that the height, area, and porosity volumetric parameters are directly known for a clastic saline reservoir. Applying the 14% efficiency factor, storage yields are 3.1 Gt and 15.8 Mt for the regional and site-specific models, respectively. Table 4 shows the range of storage potential at the P10, P50, and P90 efficiency factors for both model scales.

Table 4. CO_2 Storage Potential for the Black Island and Deadwood Formations in the Area Around the Aquistore Project

	P10	P50	P90
Efficiency Factor, %	7.4	14	24
Regional Scale	1.6 Gt	3.1 Gt	5.3 Gt
Local Scale	8.4 Mt	15.8 Mt	27.1 Mt

DYNAMIC SIMULATION

To evaluate the targeted saline system, and thus its viability as a potential sink, the geocellular model was used as the framework for an assessment of the dynamic storage capacity of the system. Static storage resource calculations do not consider the effect of dynamic factors such as injection rate, injection pattern, timing of injection, reservoir pressure buildup, and CO_2 movement for risk assessment. Numerical simulation is a method that can be used to validate the estimate of the effective storage resource potential of deep saline formations by addressing the dynamic CO_2 movement during injection.

Through the dynamic simulation effort, two main objectives were established for this project: 1) assess the dynamic storage capacity of the saline system and 2) assess the risk by simulating the reservoir performance during CO_2 injection and postinjection. To address these objectives, two dynamic injection scenarios were designed based on the static geologic model. The first scenario is used to determine the injectivity of study area through the simulated injection of 0.3 Mt/year to investigate the timing of CO_2 breakthrough in the observation well and near-wellbore CO_2 movement in a fine-scale model (13.1 mi^2). The second scenario extends the simulation to the 3670-$mile^2$ study region in an effort to optimize the injection and storage that will be included in a subsequent report. All of the dynamic simulations were performed using Computer Modelling Group Ltd.'s (CMG's) general equation-of-state modelling (GEM) software package (www.cmgl.ca/) on a 184-core, high-performance parallel computing cluster.

MODEL SETTINGS

There are two components in the model: CO_2 and brine. The CO_2 is allowed to dissolve into brine to mimic the nature of the saline system undergoing CO_2 injection. The aqueous density and viscosity of the fluids were correlated by using the Rowe and Chou (1970) and Kestin and others (1981) methods, respectively, with varying temperatures and pressures of the saline system over the location and depth. Henry's law constant was correlated by Harvey's method to determine the solubility of CO_2 in the brine (Harvey, 1996).

The fluid model and rock–fluid settings for the dynamic simulation were based on the lithologies of the static geologic model. To test the sensitivity of the system to relative permeability, three sets of the relative permeability curves were used in the simulations. The first set of relative permeability curves (RPT1) was provided by Schlumberger and was measured by an unsteady-state method from core plugs taken at depths of 10,424.9 and 10,621.7 ft which are Sample 4 and Sample 14 (Schlumberger Reservoir Laboratories, 2013). The net confining

pressure and temperature imposed to generate these measurements were 2300 psi and 104°F, respectively; however, both are lower than the reservoir conditions in the study area. The relative permeability curves of the two samples are plotted in Figure 13. The second set of curves (RPT2) was obtained from Bachu and Adams (2003) and Bachu and others (2011). From these reports the basal Cambrian sandstone, Wabamum carbonate, and shale were chosen for the simulations (Figure 14). The third set of relative permeability curves (RPT3) was fitted for the simulation based on test data generated by the EERC Applied Geology Laboratory (Figure 15). The sample tested was taken from a core plug obtained from a depth of 10,859.9 ft, with the average porosity of 6.3% and a permeability of 4.89 mD. The pressure and temperature conditions for the sample test were 4000 psi and 176°F, respectively.

NUMERICAL TUNING

A numerical tuning technique was used to optimize the numerical settings for increasing the speed of the simulation runs. Various parameters such as pressure change and the tolerance of convergence over each time step were tracked to tune the integrated settings for producing the lowest optimization critical points (Griffith and Nichols, 1996; Hutchinson, 1989; LeDimet and others, 1995). The optimization critical points used in the project included material balance error, central processing unit (CPU) time, and solver failure percent. After numerical tuning, up to a 35% reduction in run time was achieved.

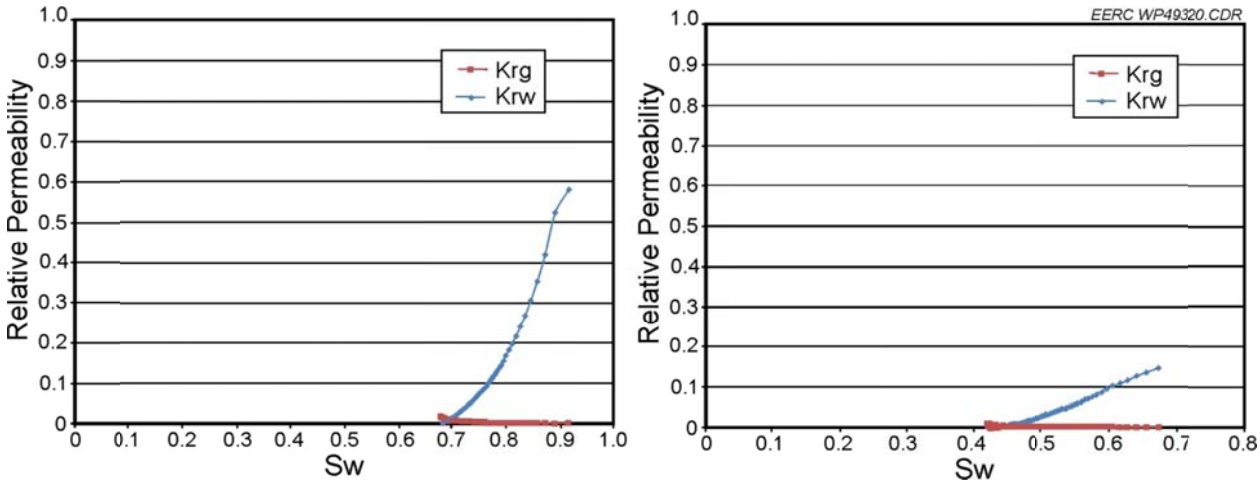

Figure 13. Relative permeability curves for the two samples (Schlumberger Reservoir Laboratories, 2013).

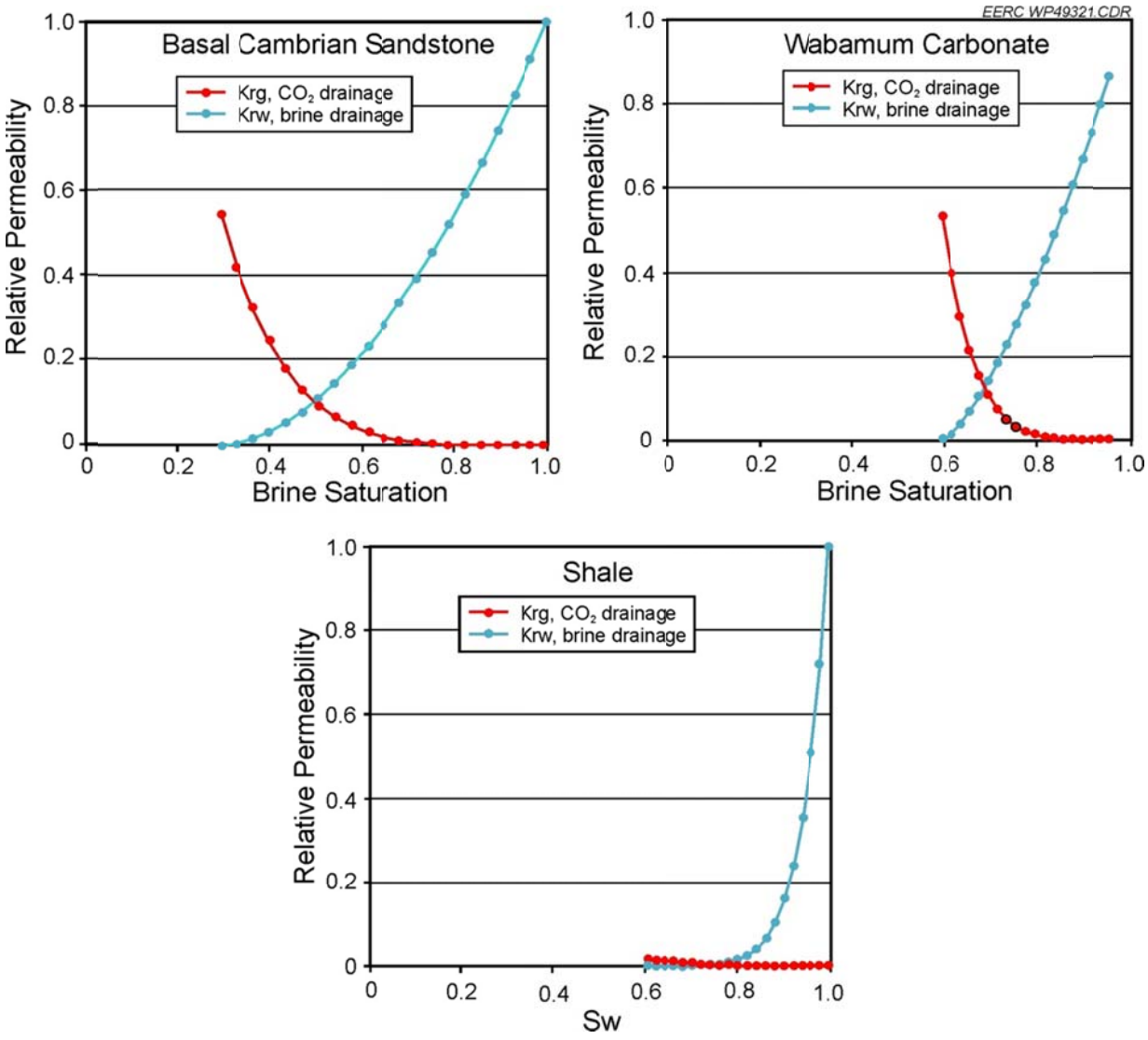

Figure 14. Relative permeability curves used for the simulation (Bachu and Adams, 2003; Bachu and others, 2011).

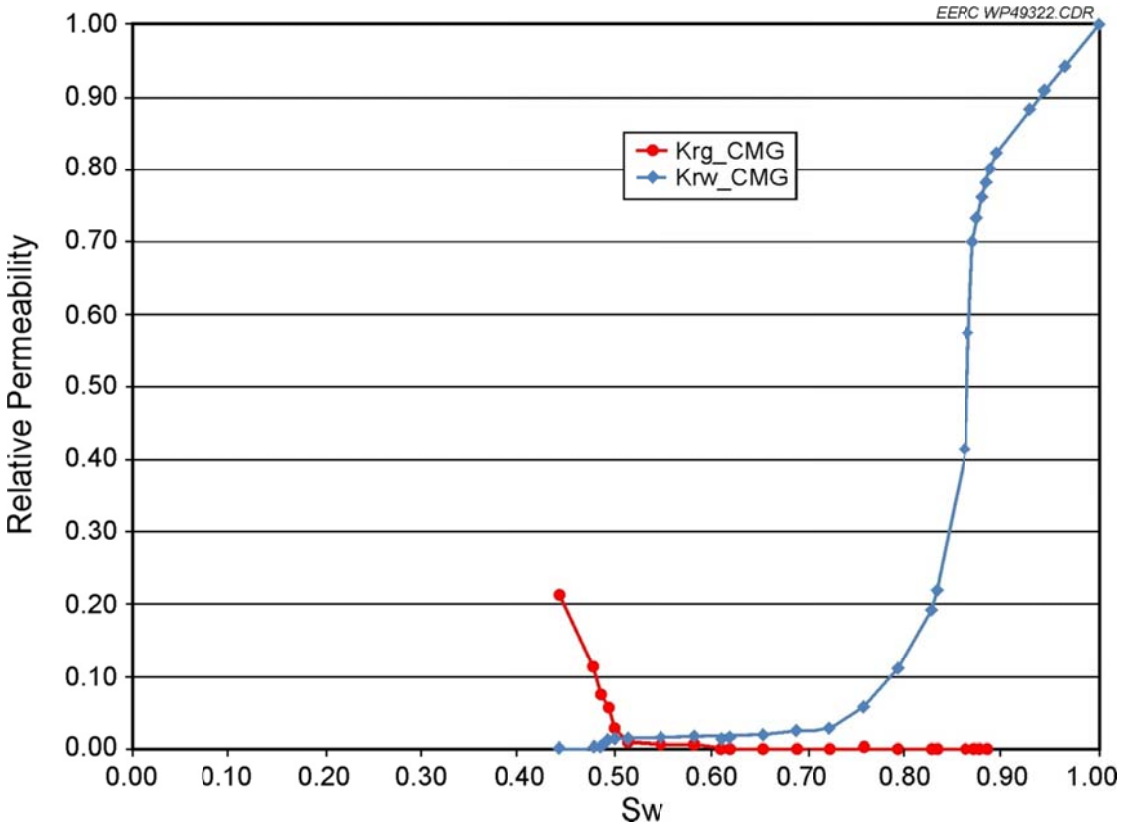

Figure 15. Relative permeability fitted for the CMG simulation based on data tested by the EERC Applied Geology Laboratory.

SIMULATION RESULTS AND DISCUSSION

A total of nine cases were designed to address dynamic CO_2 storage capacity based on various factors, including boundary conditions, injection rates and periods, and relative permeabilities as listed in Table 4. In addition to variations in a long-term scenario of 1 Mt/yr for 50 years, a smaller volume (0.3 Mt/yr) and shorter time periods (1 and 5 years) were also simulated. These lower values were chosen to more closely replicate the expected injection design at the Aquistore site and to better investigate the CO_2 movement to and breakthrough at the observation well. Moreover, reservoir pressure differences during injection and postinjection were evaluated to improve the risk assessment and improve the MVA process.

50-year Injection Period

The cases with 50-year injection periods were used to determine CO_2 storage potential based on the high injection rate for a relatively long time period. The potential storage capacity depended on factors such as rock properties and boundary conditions (Table 5). There is a large range of injection totals for the 50-year scenarios, shown in Table 5. With respect to Cases 1 and 2, the 4× increase is directly related to the variability in relative permeability values

Table 5. Results Summary for Nine Cases by Varying Simulation Factors

Case	Boundary Conditions	Injection Rate, Mt/year	Injection Period, years	Relative Permeability	Total Injected CO_2, Mt
1	Closed	1	50	RPT 1	1.505
2	Closed	1	50	RPT 2	6.337
3	Opened	1	50	RPT 2	33.652
4	Opened	1	5	RPT 2	3.663
5	Opened	1	1	RPT 2	0.671
6	Opened	0.3	5	RPT 2	1.593
7	Opened	0.3	5	RPT 3	1.465
8	Opened	0.3	1	RPT 2	0.290
9	Opened	0.3	1	RPT 3	0.286

(Table 5 and Figures 16 and 17). The even larger change from Case 2 to Case 3 is entirely related to the change in boundary conditions between the two cases. The open boundary scenario allowed aquifer communication outside of the model bounds. Because of the geologic characterization, it is expected that the Aquistore site will behave as an open system. However, the two closed-system cases were run to investigate the absolute minimum injectivity and capacity of the site.

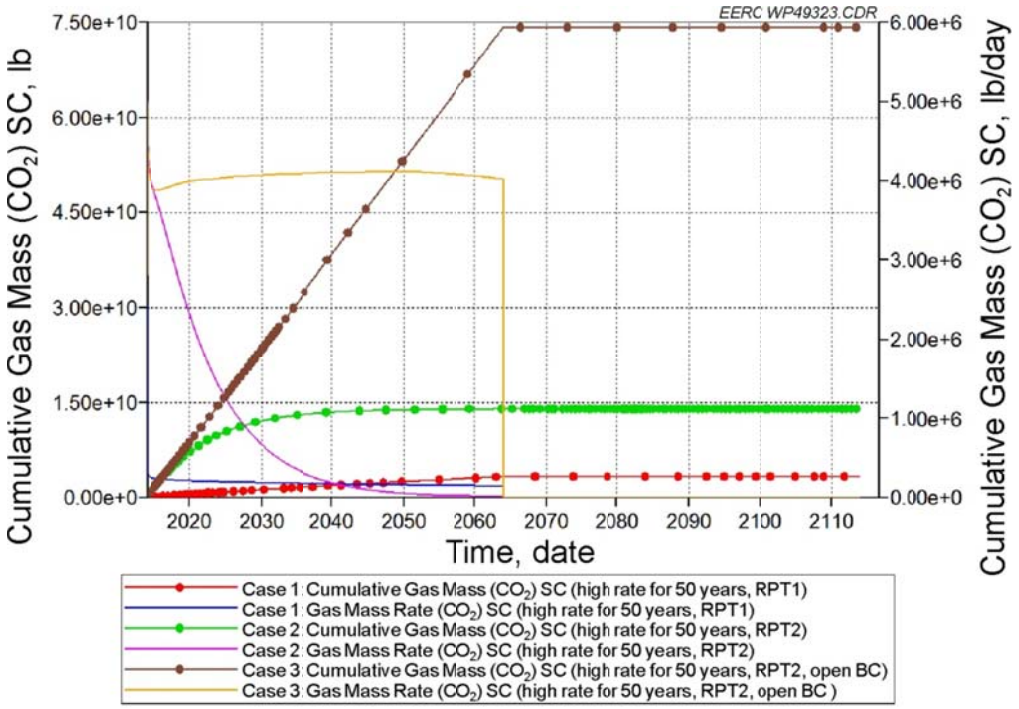

Figure 16. Total injected CO_2 and real injection rate for Cases 1–3.

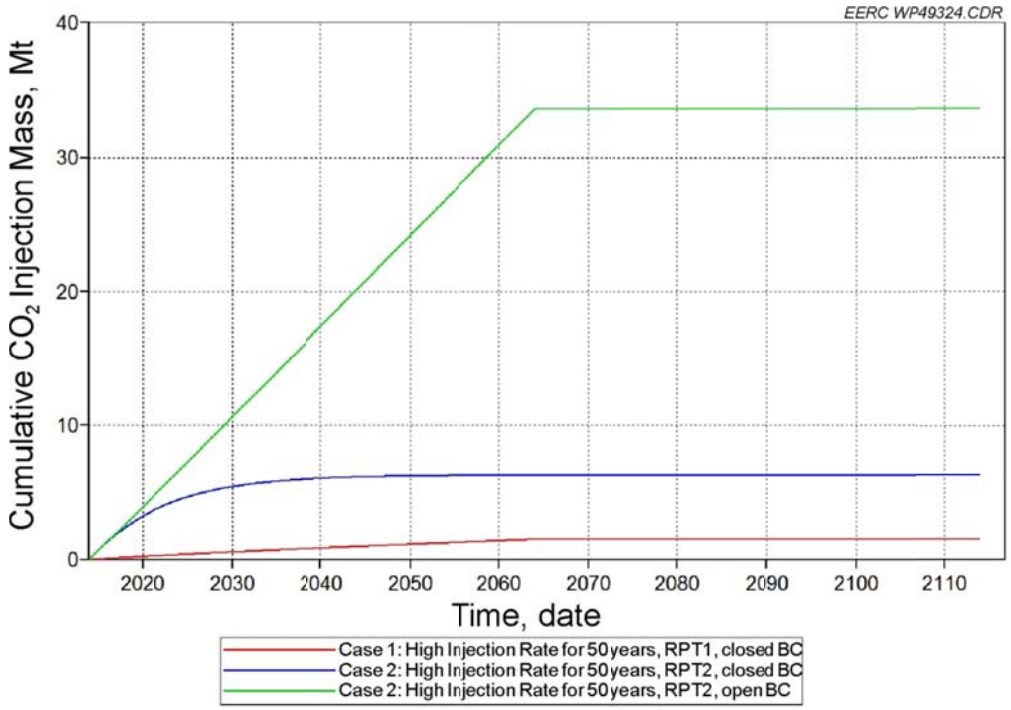

Figure 17. Total injected CO_2 by mass for Cases 1 and 2.

5-year and 1-year Injection Periods

High Injection Rate vs. Low Injection Rate

Although the maximum injection rate was set as 1 Mt/year, the simulated maximum injection rate for Cases 4 and 5 was about 0.73 Mt/year under the maximum bottomhole pressure constraint of 6200 psi, which is 90% of the tested fracture pressure (Peck, 2013) (Table 5 and Figure 18). This constraint is the main reason the total injected CO_2 in Cases 4 and 5 is less than might be expected at the 1-Mt/year injection rate. However, the expected injection rate of 0.3 Mt/yr, in Cases 6–9 are close to the expected amount of CO_2 under the same bottomhole pressure constraint (Table 5 and Figures 19 and 20). In other words, it is very likely that the 0.3 Mt/yr could be injected through one well at the Aquistore site and, potentially, up to 0.73 Mt/yr.

5-year Injection Period vs. 1-year Injection Period

The total injected CO_2 results for the 5-year period are close to five times higher than the results for the 1-year injection period. However, the longer-injection-period cases show approximately 9% more than five times the 1-year period results because of open boundary effects (Table 5 and Figures 19 and 20).

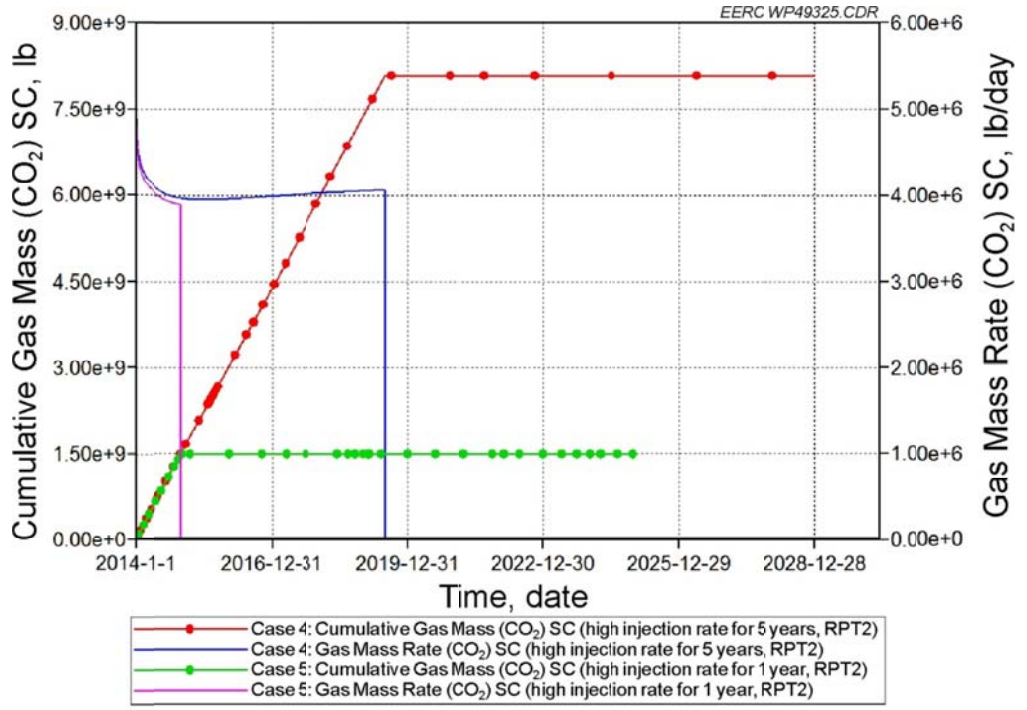

Figure 18. Total injected CO_2 and injection rate for Cases 4 and 5.

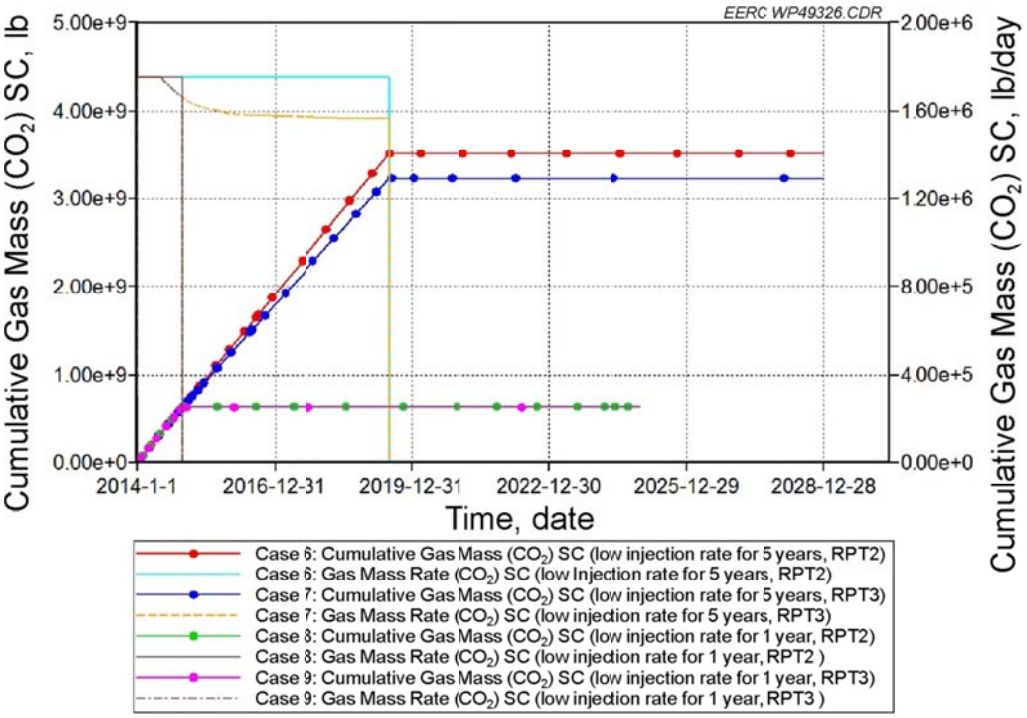

Figure 19. Total injected CO_2 and injection rate for Cases 6–9.

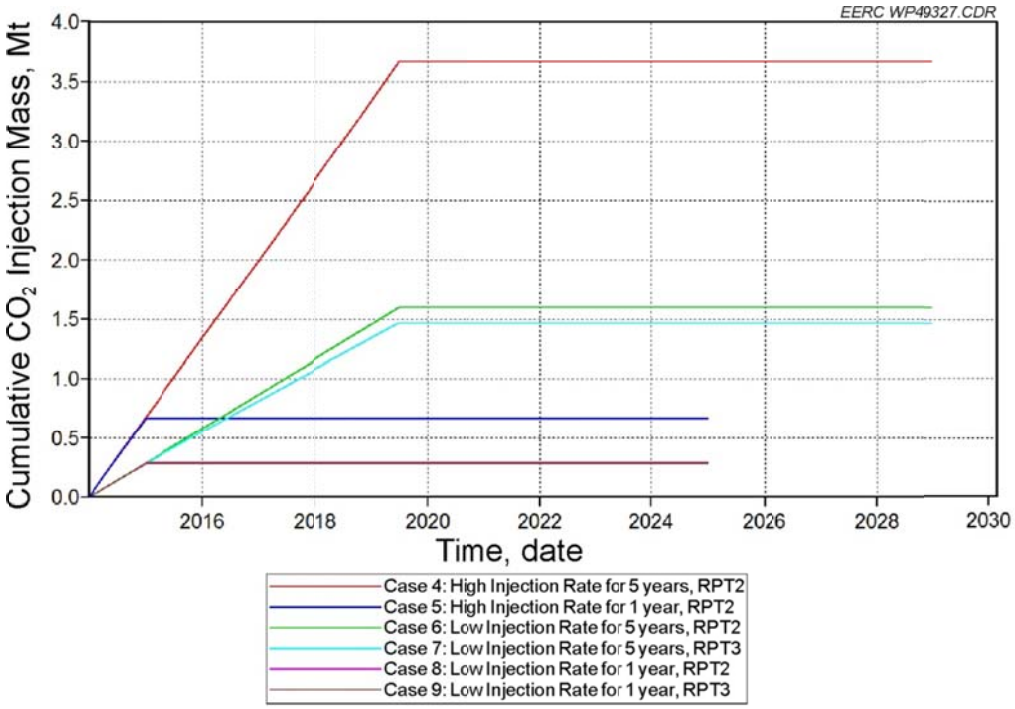

Figure 20. Total injected CO_2 by mass for Cases 4–9.

Relative Permeability Sensitivity

Relative permeability values from Bachu and Adams (2003) and Bachu and others (2011), along with values derived from the EERC Applied Geology Laboratory (Figure 3), were applied to the 1-year and 5-year injection period cases. The total injected CO_2 with relative permeability values from the EERC, is generally lower than the cases using the data from Bachu and Adams (2003) and Bachu and others (2011), especially in the longer injection periods (Table 5 and Figures 19 and 20). For example, the total injected CO_2 is about 1% lower in Case 9 than the results in Case 8 for 1-year injection, and this difference increases to 9% with 5 years of injection in Cases 6 and 7 (Table 5 and Figures 19 and 20). The main reason for this difference is that both residual water saturation and overall relative permeability from the EERC-derived data are lower than the curves from Bachu and Adams (2011) (Figures 2 and 3). Moreover, the concentrations of CO_2 in the plumes created using EERC-derived relative permeability are different because of the residual gas and water values (Figures A-7–A-9, Appendix A).

CO_2 Breakthrough to the Observation Well

From a monitoring standpoint, CO_2 breakthrough time at the observation well was investigated in both a high (1 Mt/yr) and low injection rate (0.3 Mt/yr) scenario. The earliest CO_2 breakthrough occurred between 10 and 15 days after injection began in the 1-Mt/yr injection rate scenarios. The CO_2 breakthrough occurred in the top reservoir zone of the Deadwood Formation in Cases 4 and 5 (Figure 21). With the lower injection rate of 0.3 Mt/year in Cases 6 and 8, the earliest simulated CO_2 breakthrough occurred between 25 and 30 days after injection began and broke through along the same reservoir zone of the formation (Figure 22).

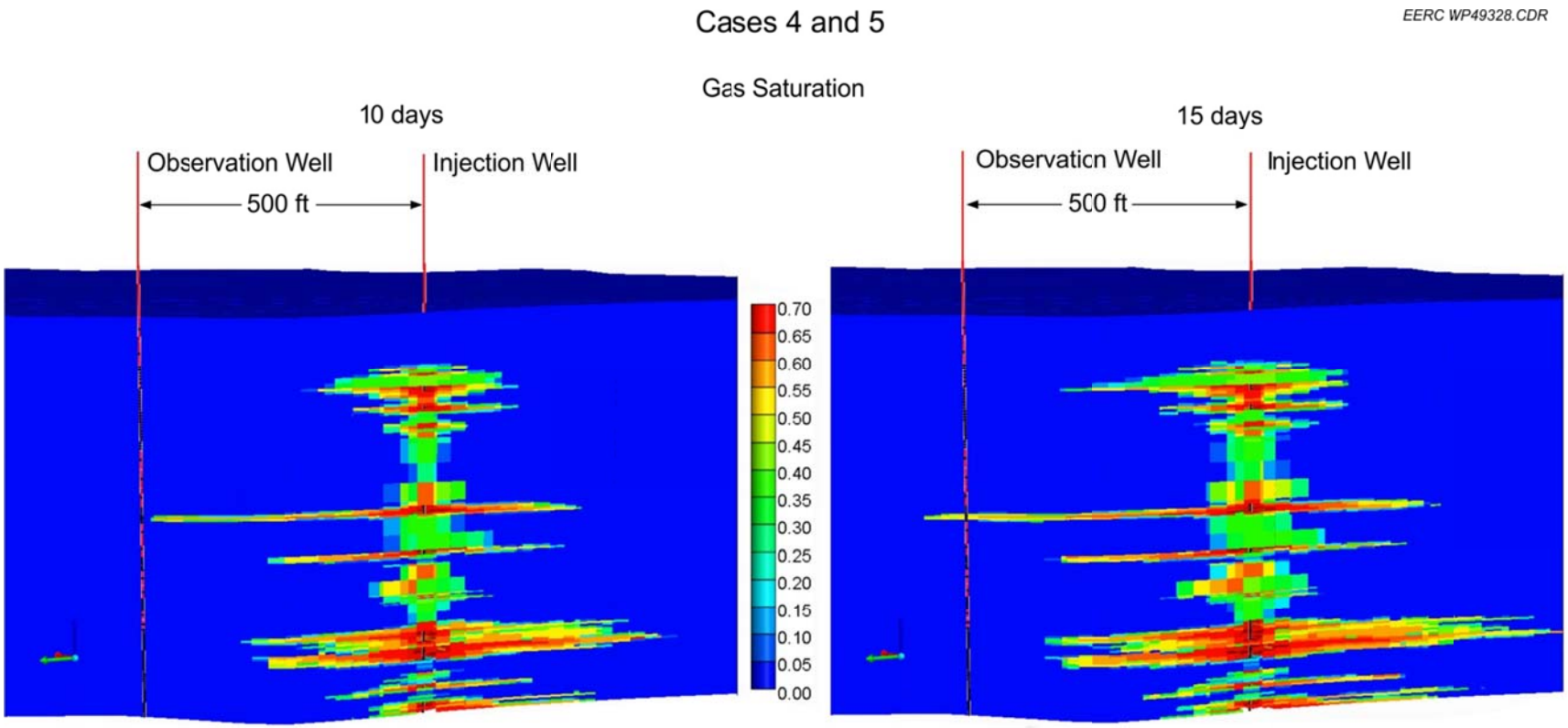

Figure 21. Cross-sectional view of CO_2 breakthrough in Cases 4 and 5 with high injection rate (1 Mt/year). The earliest breakthrough between 10 and 15 days after injection that happened in the top reservoir zone of the Deadwood Formation.

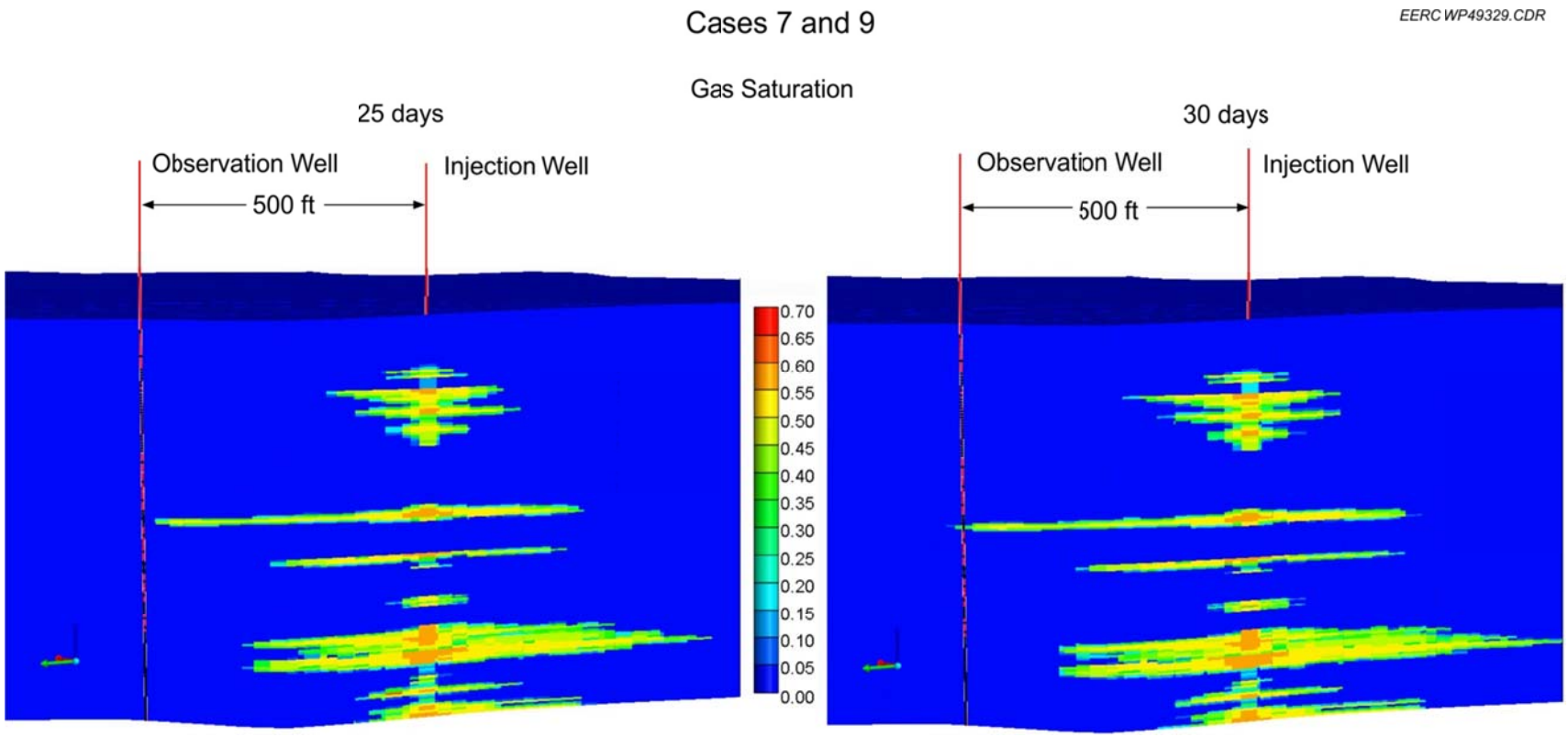

Figure 22. Cross-sectional view of CO_2 breakthrough in Cases 6 and 8 with low injection rate (0.3 Mt/year). The earliest breakthrough between 25 and 30 days after injection happened in the top reservoir zone of the Deadwood Formation.

Although the relative permeability used in Cases 7 and 9 was from Bachu and Adams (2011) based on the data derived by the EERC Applied Geology Laboratory, the earliest CO_2 breakthrough still happened between 25 to 30 days after injection, similar to the cases based on relative permeability (Figure 23). Based on the information derived from the simulation cases, the CO_2 breakthrough will most likely happen in the first month of injection, regardless of the injection rate and assumptions of relative permeability.

The primary reason for the relatively short breakthrough time is that the distance between the injection well and the observation well is only about 500 ft, and these points are well connected via the permeable upper Deadwood sand. More detailed results of CO_2 breakthrough in the other reservoir zones and the shape of the CO_2 plume over time can be found in Appendix A (Figures A-1–A-10).

Pressure Differences

The pressure difference discussed in this report was calculated by the pressure at the specific time in the simulation minus the initial pressure to check how much pressure changed during CO_2 injection or postinjection. Overall, the maximum simulated pressure difference was 1700 psi in Case 2 with closed boundary conditions, and this value reduces to about 900 psi with the open boundary system in Case 3 (Figure A-3, Appendix A). For Case 4 with 5 years of injection, the pressure difference is about 1000 psi at the end of injection, and this value decreases to 90 psi after 5 years of postinjection (Figure A-6, Appendix A). The results of Case 5 also show the same trend, but the pressure difference is smaller since the injection duration is only 1 year (Figure A-6, Appendix A). The reservoir pressure changes due to CO_2 injection are still limited by the fracture pressure in these simulations, and the pressure differences dissipate very quickly during the years of postinjection, especially for the cases with short injection durations.

CONCLUSIONS AND FUTURE WORK

Based on the simulation results, the storage of CO_2 in the study area using the existing two-well configuration is feasible, depending on the volume of CO_2 available from the Boundary Dam power plant. The static CO_2 capacity for the local- or fine-scale model extent ranges from 8.4 Mt to 27.1 Mt for the P10 and P90 confidence levels, respectively. With regard to a dynamic storage capacity, the maximum simulated injectivity for the current injection well is 0.73 Mt/year based on the geologic characterization of the study area. Based on these simulation results, the maximum storage potential of the Aquistore site with one injection well is approximately 34 million tons after 50 years. However, this can be improved based on optimization operations such as multiple injectors, formation water extraction, and horizontal injection, which will be investigated in the next phase. The larger capacity value obtained through the dynamic modeling suggests that the storage coefficient used in the static approach may be too low and that the CO_2 will successfully interact with a larger percentage of the system.

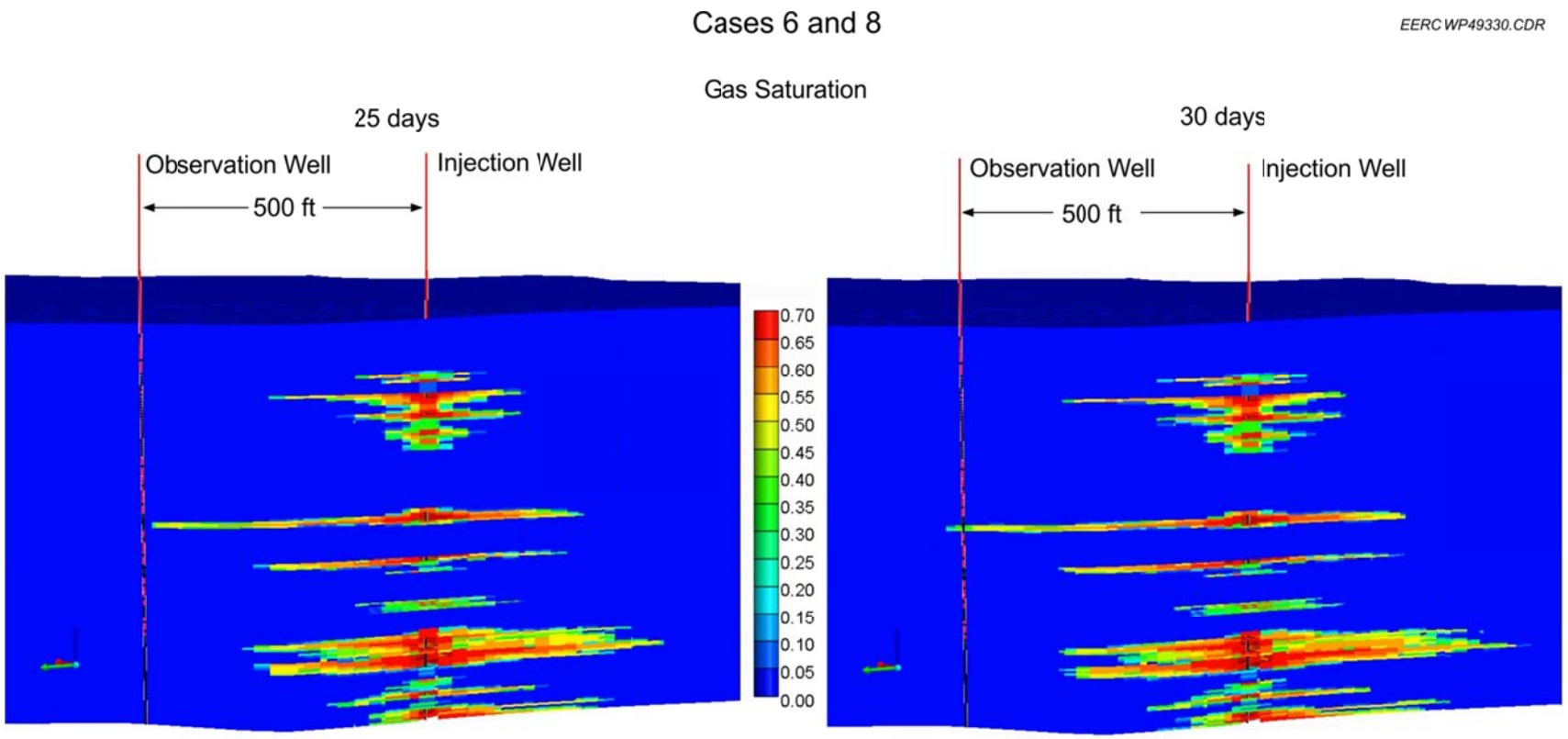

Figure 23. Cross-sectional view of CO_2 breakthrough in Cases 7 and 9 with low injection rate (0.3 Mt/year) utilizing the relative permeability tested by the EERC Applied Geology Laboratory. The earliest breakthrough between 25 and 30 days after injection happened in the top reservoir zone of the Deadwood Formation.

Boundary conditions of the model play a significant role in the estimation of CO_2 storage capacity. Specifically, with an open system configuration that allows fluid and pressure communication up to and beyond the model boundaries, there is the potential for greater storage capacity/efficiency. It is currently expected that the system is open; however, further geological investigation will be help to properly identify and extend the open system from the small area to the extended region.

Based on the simulated CO_2 injection cases, the earliest CO_2 breakthrough to the observation well may happen in as few as 15 days with a 1-Mt/year injection rate. The breakthrough time at the observation well may be extended to 1 month if the injection rate is reduced to 0.3 Mt/yr. The simulated overall CO_2 breakthrough in the other reservoir zones occurred after about 3 months of injection with the low injection rate, and this breakthrough time was reduced to about 45 days at the high injection rate.

The simulated pressure response in all cases indicated that the system was locally pressure-limited in the open-system cases, as an injection rate of 1 Mt/yr was not achieved in any case. In the closed-system cases, pressure was also limited by boundary conditions, which resulted in a much lower injection rate.

Future work will include extending the size of the model to provide better insights with respect to a commercial-scale rate of injection over a long period of time. In addition, geotechnical, geochemical, and geothermal behaviors will be integrated throughout the entire modeling and simulation process to investigate the role of these variables in the overall storage estimation. In addition, more core analysis data will be integrated into the modeling and simulation to reduce uncertainty, and the actual injection volumes will be modeled once injection begins at the site.

ACKNOWLEDGMENTS

The authors extend thanks and recognition to PTRC and, specifically, Neil Wildgust and Kyle Worth for sharing detailed geologic information related to the injection and observation wells drilled for the Aquistore project. We also thank Schlumberger Carbon Services for providing its base model for our use and review and Wade Zaluski of Schlumberger for providing access to the Aquistore core as well as core plugs for our testing and examination.

REFERENCES

Bachu, S., and Adams, J. J., 2003, Sequestration of CO_2 in geological media in response to climate change—capacity of deep saline aquifers to sequester CO_2 in solution: Energy Conversion and Management, v. 44, no. 20, p. 3151–3175.

Bachu, S., Faltinson, J., Hauck, T., Perkins, E., Peterson, J., Talman, S., and Jensen, G., 2011, The Basal Aquifer in the Prairie region of Canada—characterization for CO_2 storage: Preliminary report for Stage I (Phases 1 and 2), Alberta Innovates Technology Futures.

Goodman, A., Hakala, A., Bromhal, G., Deel, D., Rodosta, T., Frailey, S., Small, M., Allen, D., Romanov, V., Fazio, J., Huerta, N., McIntyre, D., 2011, U.S. Department of Energy methodology for the development of geologic storage potential for carbon dioxide at the national and regional scale: International Journal of Greenhouse Gas Control, v. 5, no. 4, p. 952–965.

Gorecki, C.D., Liu, G., Bailey, T.P., Sorensen, J.A., Klapperich, R.J., Braunberger, J.R., Steadman, E.N., and Harju, J.A., 2013, The role of static and dynamic modeling in the Fort Nelson CCS Project: Energy Procedia v. 37, p. 3733–3741, ISSN 1876-6102, http://dx.doi.org/10.1016/j.egypro.2013.06.268.

Gorecki, C.D., Sorensen, J.A., Bremer, J.M., Knudsen, D.J., Smith, S.A., Steadman, E.N., and Harju, J.A., 2009, Development of storage coefficients for determining the effective CO_2 storage resource in deep saline formations: SPE Paper 126444, SPE International Conference on CO_2 Capture, Storage, and Utilization, San Diego, November 2–4, 2009.

Griffith, A., and Nichols, N., 1996, Accounting for model error in data assimilation using adjoint methods, in Computational Differentiation: Techniques, Applications and Tools, Proceedings.

Harvey, A.H., 1996, Semiempirical correlation for Henry's Constants over large temperature ranges: American Institute of Chemical Engineers Journal, v. 42, p. 1491.

Hutchinson, M., 1989, A stochastic estimator of the trace of the influence matrix for Laplacian smoothing splines. Communication in Statistics – Simulation and Computation, v. 19, no. 2, p. 433–450.

Kestin, J., Khalifa, H.E. and Correia, R.J. 1981. Tables of Dynamic and Kinematic Viscosity of aqueous NaCI solutions in the temperature range 20°–150°C and the pressure range 0.1–35 MPa: Journal of Physical and Chemical Reference Data, v. 10, p. 71–87.

LeDimet, F., Ngodock, H., and Navon I., 1995, Sensitivity analysis in variational data assimilation: Supercomputer Computations Research Institute Technical Report, FSU-SCRI-95T-103, Tallahassee, Florida, The Florida State University.

Peck, W., 2013, Personnel communication with Petroleum Technology Research Centre.

Rowe, A.M., and Chou, J.C.S., 1970, Pressure–volume–temperature-concentration relation of aqueous NaCl solutions: Journal of Chemical Engineering Data, v. 15, no. 1, p. 61–66.

Schlumberger Reservoir Laboratories, 2013, Relative permeability by unsteady-state method: Prepared for Petroleum Technology Research Centre, Well: 5-6-2-8, Regina, Saskatchewan.

U.S. Department of Energy Office of Fossil Energy, 2010, Carbon sequestration atlas of the United States and Canada, 3rd edition.

APPENDIX A

SIMULATION RESULTS OF CO_2 MOVEMENT AND PRESSURE DIFFERENCE OVER TIME

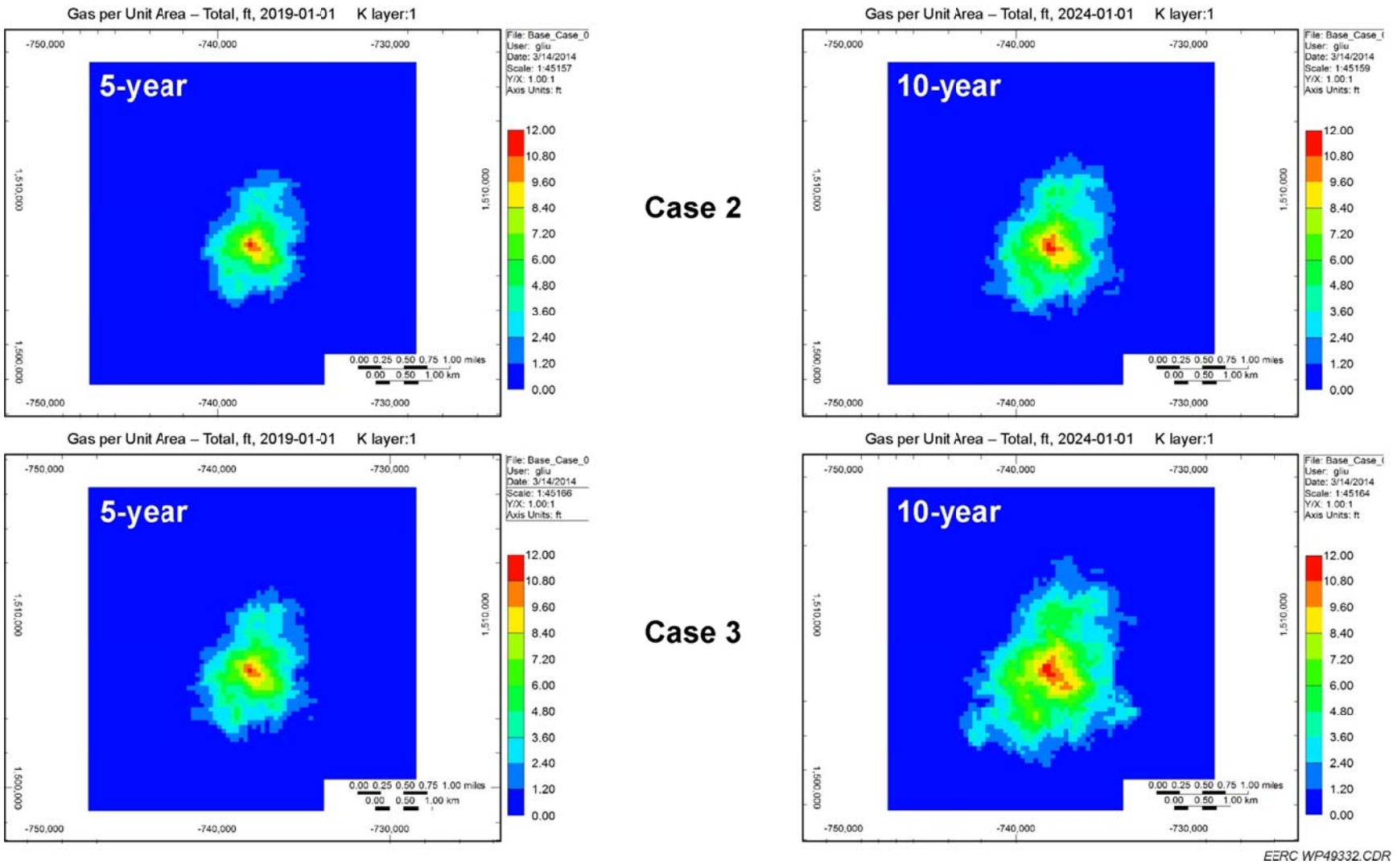

Figure A-1. Plane view of CO_2 plume comparison between Cases 2 and 3 over time based on the closed and open boundary conditions.

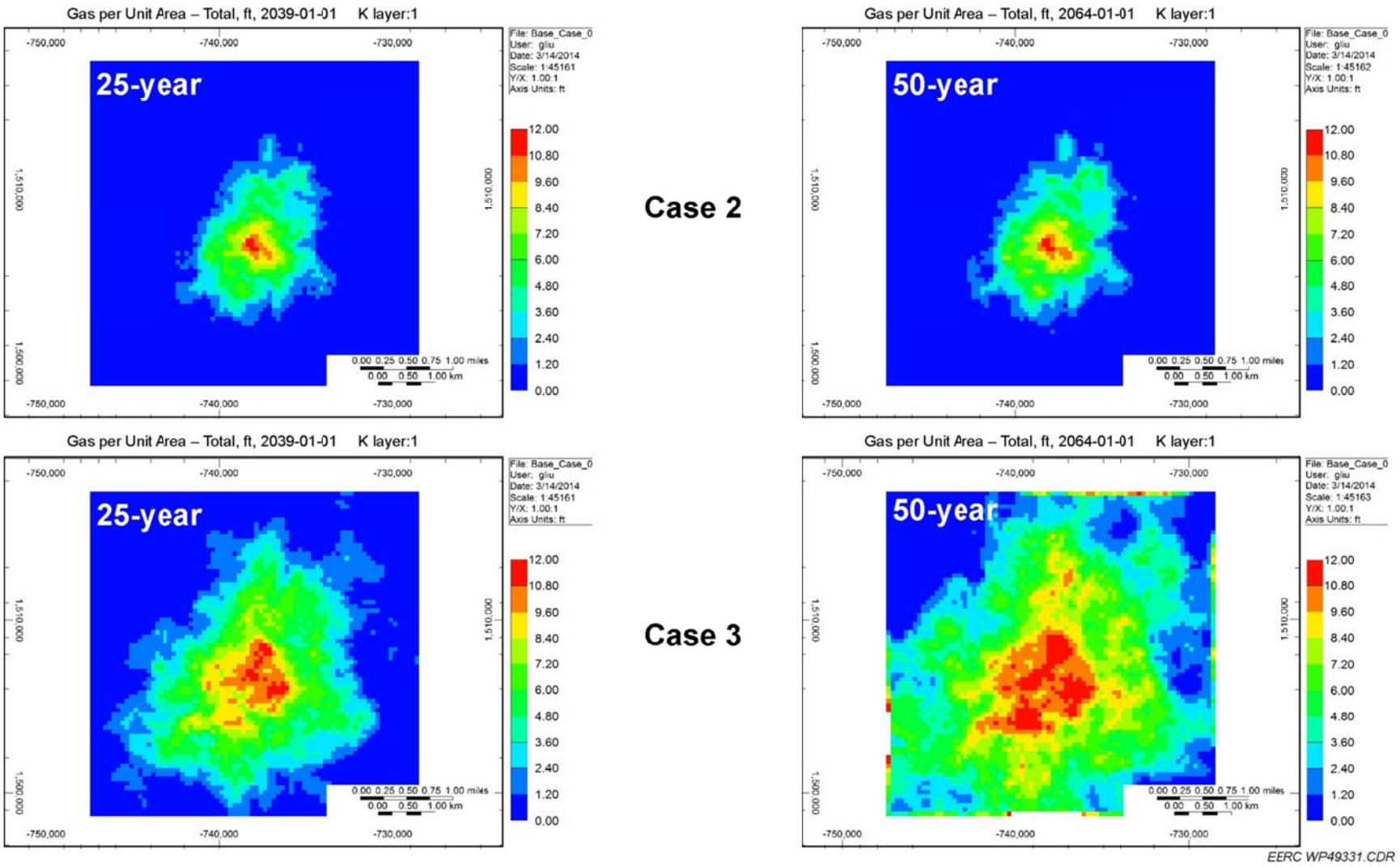

Figure A-2. Plane view of CO_2 plume comparison between Cases 2 and 3 over time based on the closed and open boundary conditions.

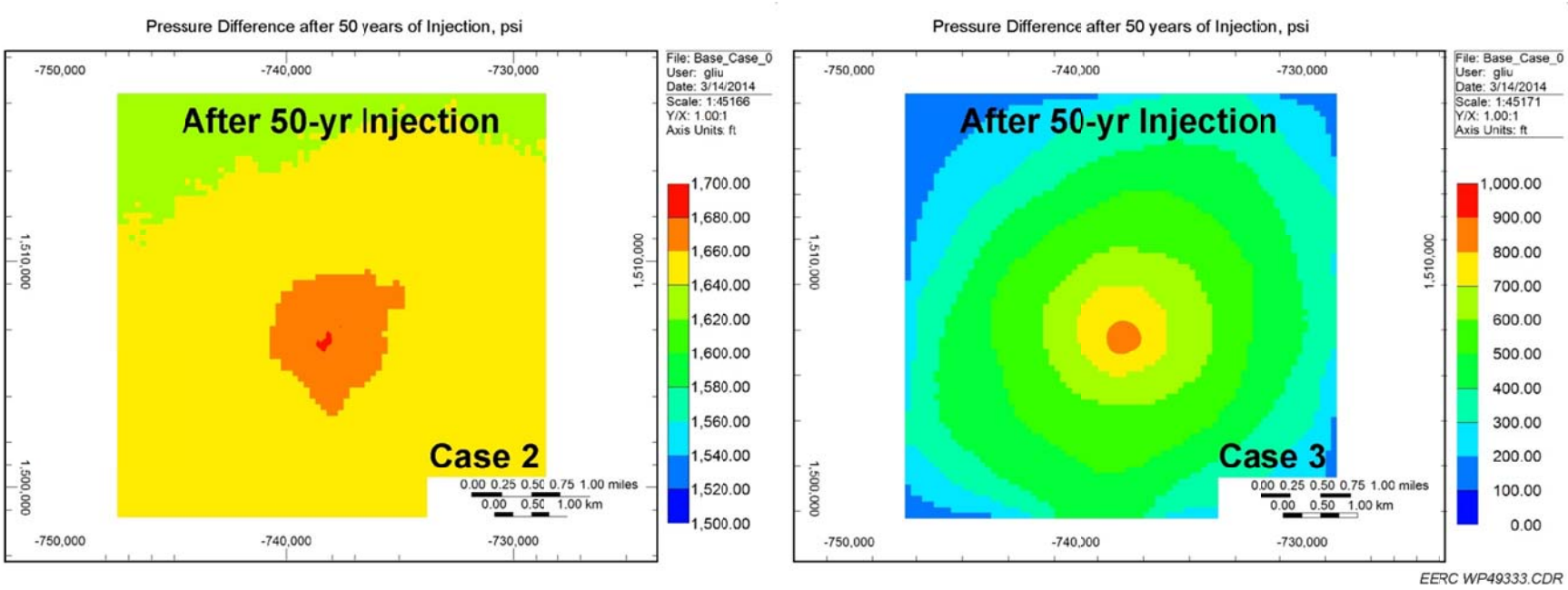

Figure A-3. Plane view of pressure difference comparison between Cases 2 and 3 over time based on the closed and open boundary conditions. The pressure difference of Case 2 with closed boundary settings is about 1600 to 1680 psi after 50-year injection, and the values reduce to the range of 100 to 900 psi in Case 3 with open boundary conditions.

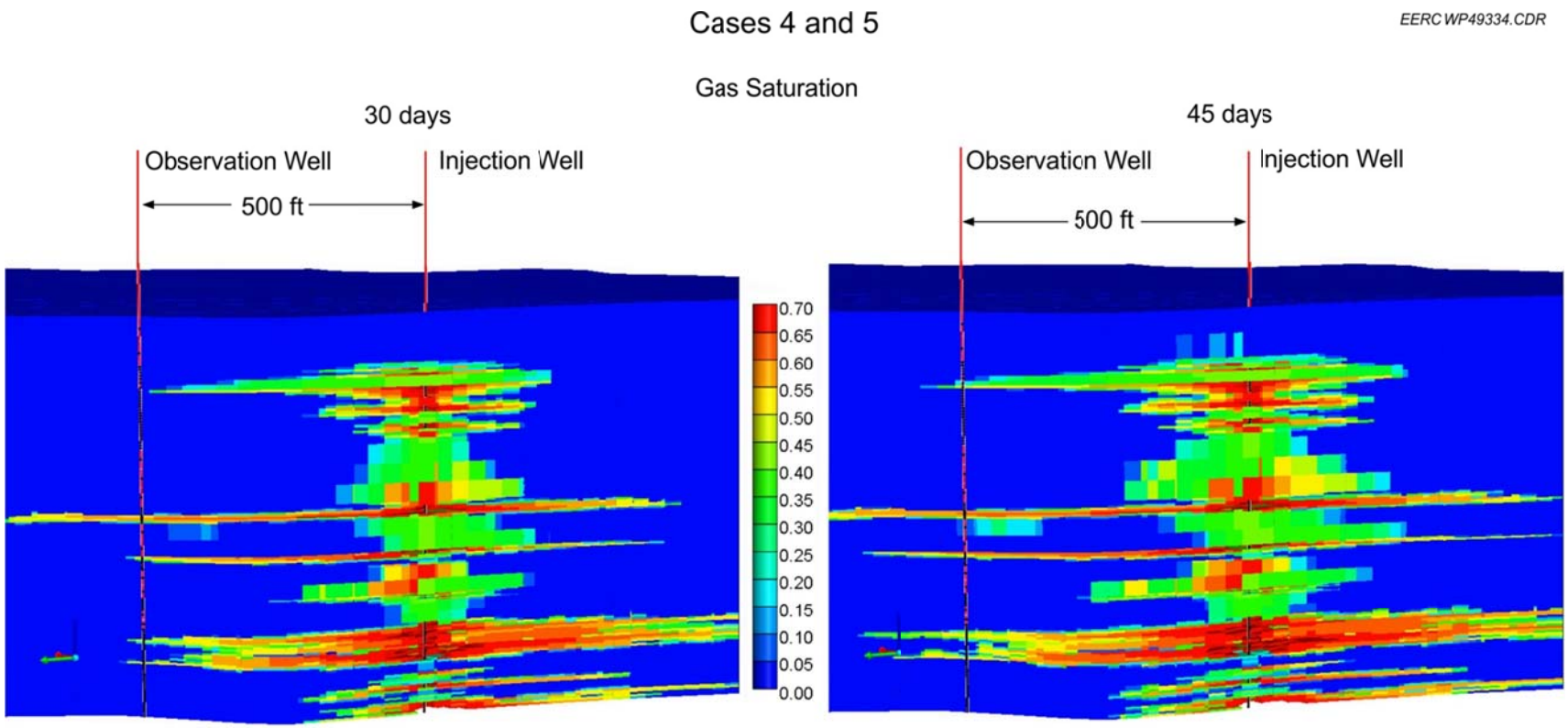

Figure A-4. Cross-sectional view of CO_2 breakthrough at the observation well in Cases 4 and 5 with high injection rate, 1 Mt/year over 30 days and 45 days. After 45 days of injection, the CO_2 breakthrough happened in most reservoir zones.

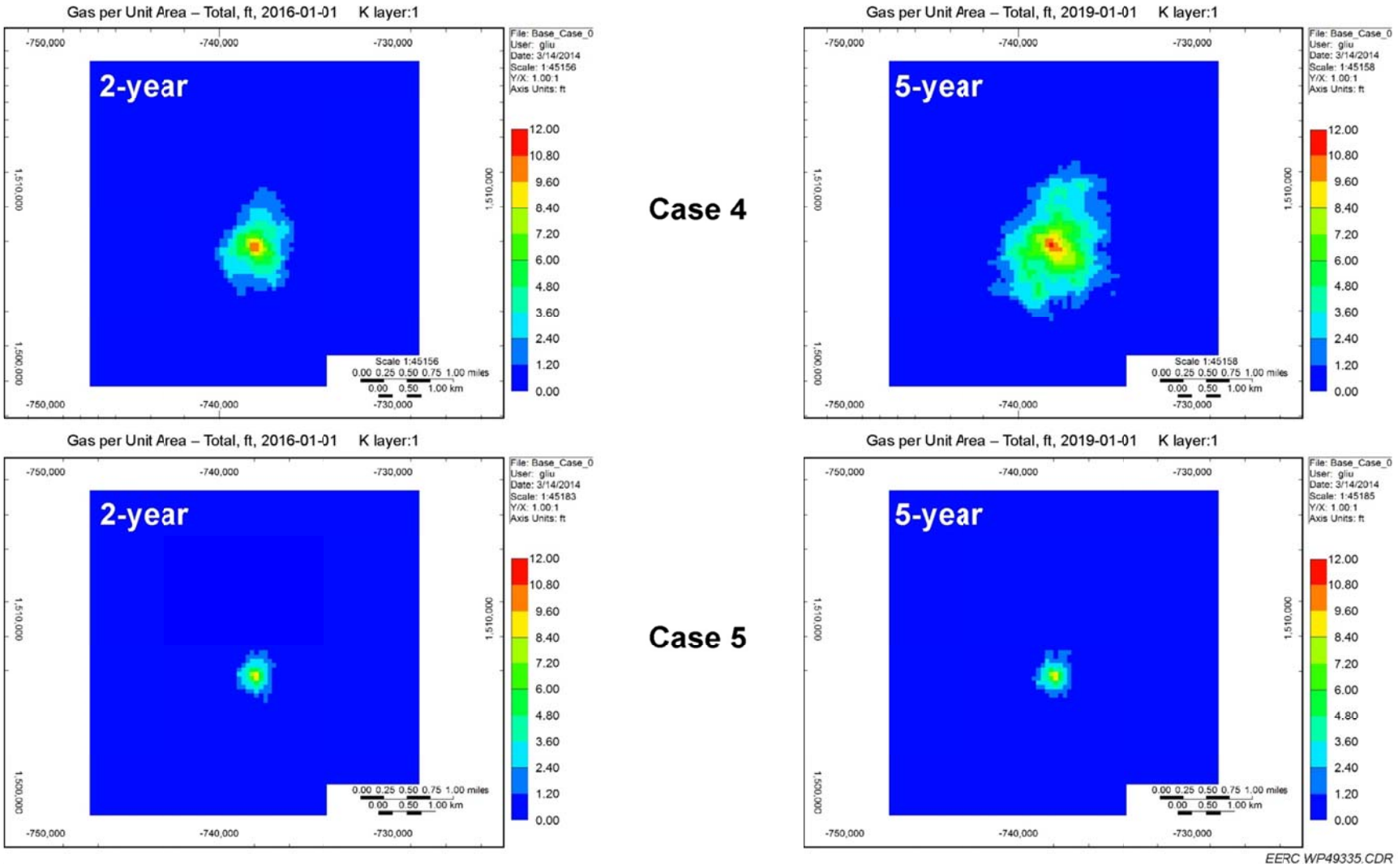

Figure A-5. Plane view of CO_2 plume with high injection rate, 1 Mt/year in Case 4 for 1-year injection and Case 5 for 5-year injection periods.

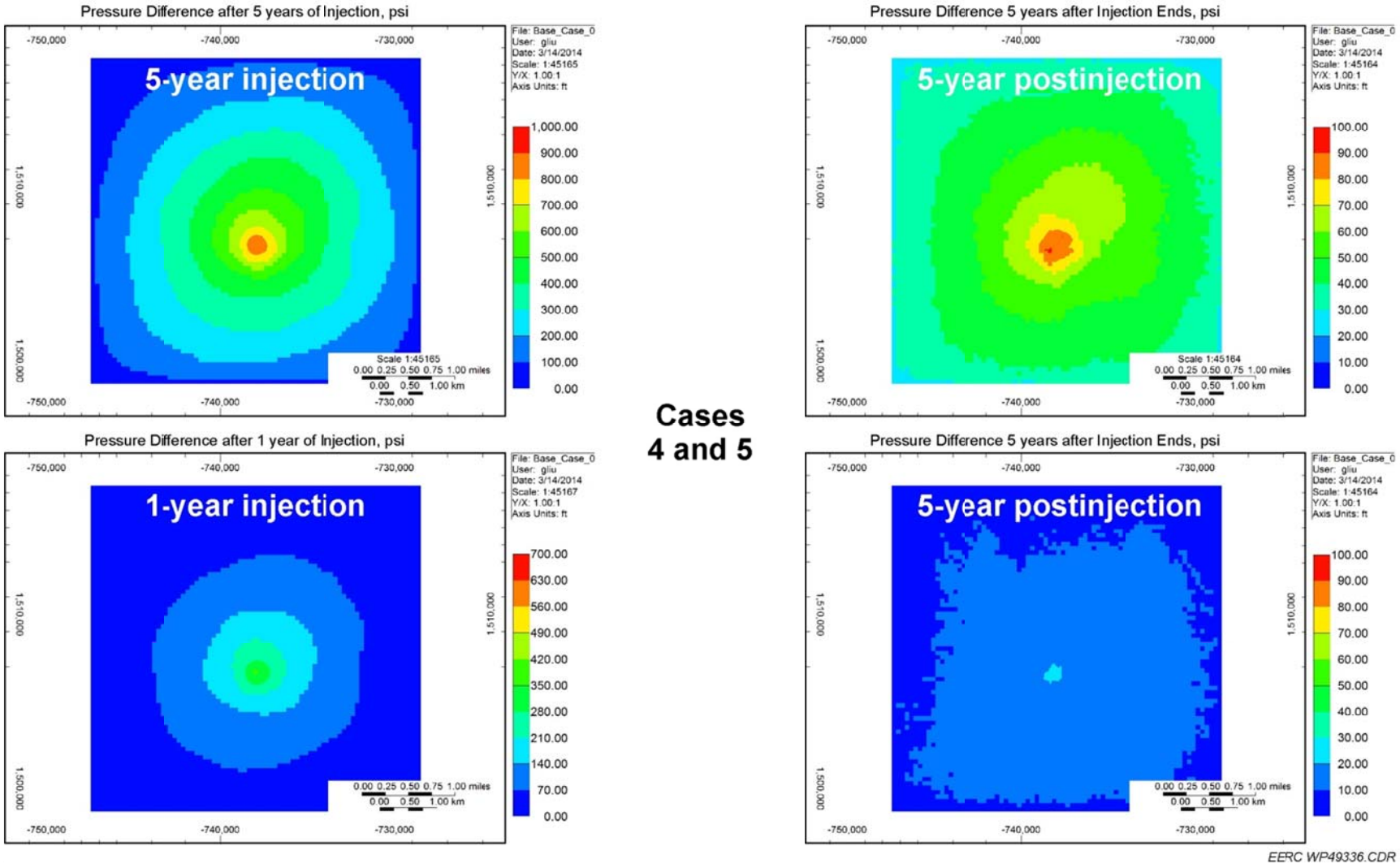

Figure A-6. Plane view of pressure difference comparison between Cases 4 and 5 over time. The maximum pressure difference of Case 4 with 5 years of injection is about 1000 psi, and the values reduce to 90 psi after 5 more years of dissipation (postinjection); the values for Case 5 with 1-year injection are 800 psi at the time injection stops and 40 psi after 5 years postinjection.

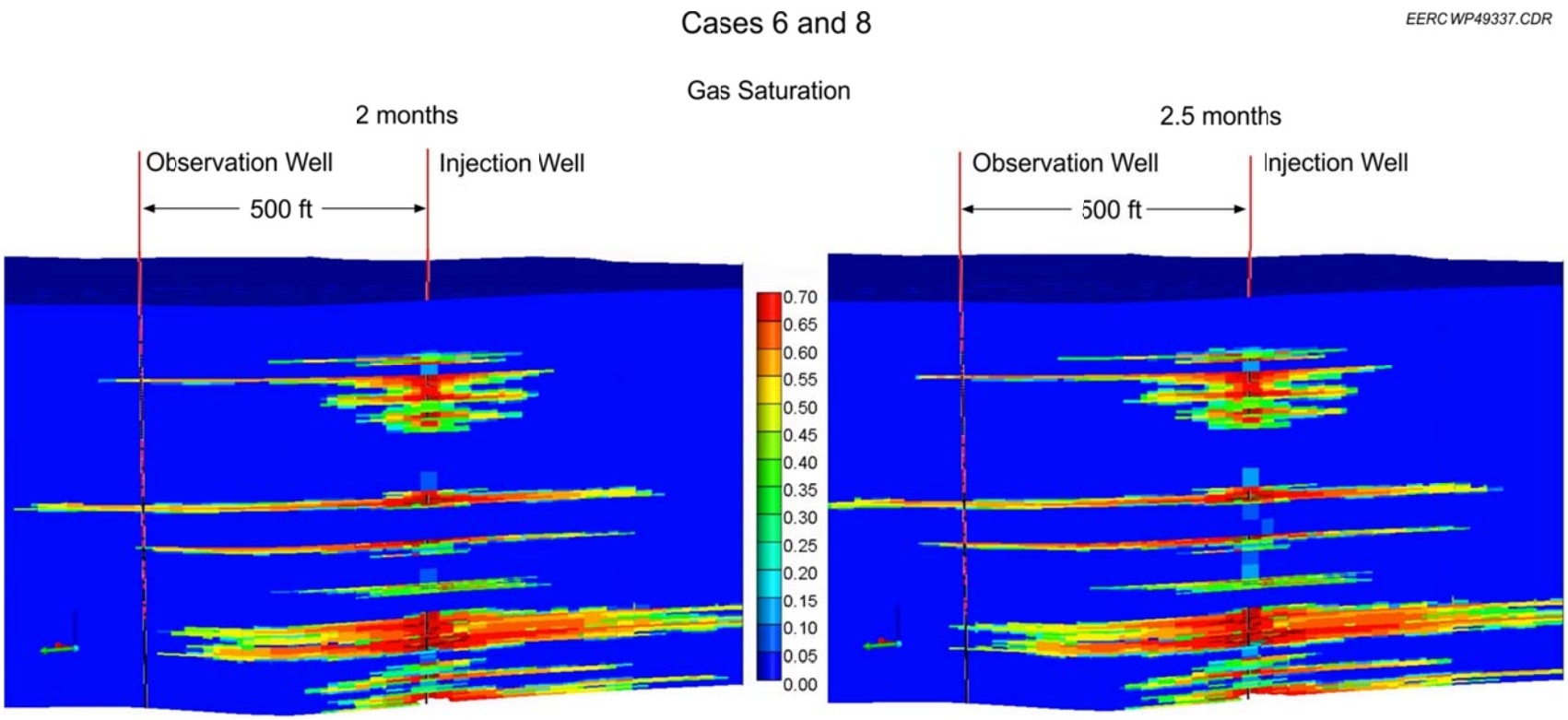

Figure A-7. Cross-sectional view of CO_2 breakthrough at the observation well in Cases 6 and 8 with low injection rate, 0.3 Mt/year over 2 months and 3 months. After 3 months of injection, the CO_2 breakthrough happened in most reservoir zones.

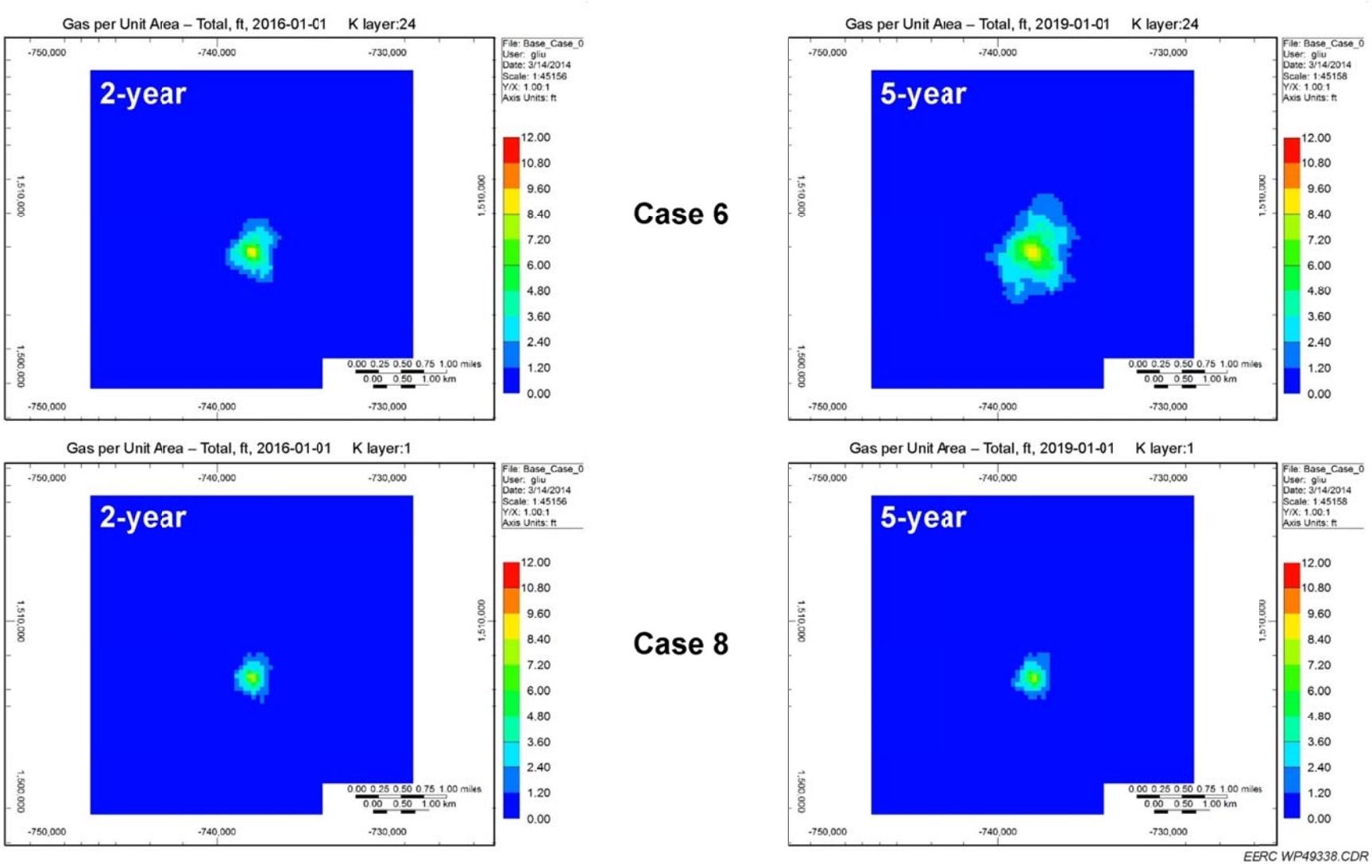

Figure A-8. Plane view of CO_2 plume with low injection rate, 0.3 Mt/year in Cases 6 and 8 after 2 years and 5 years of injection.

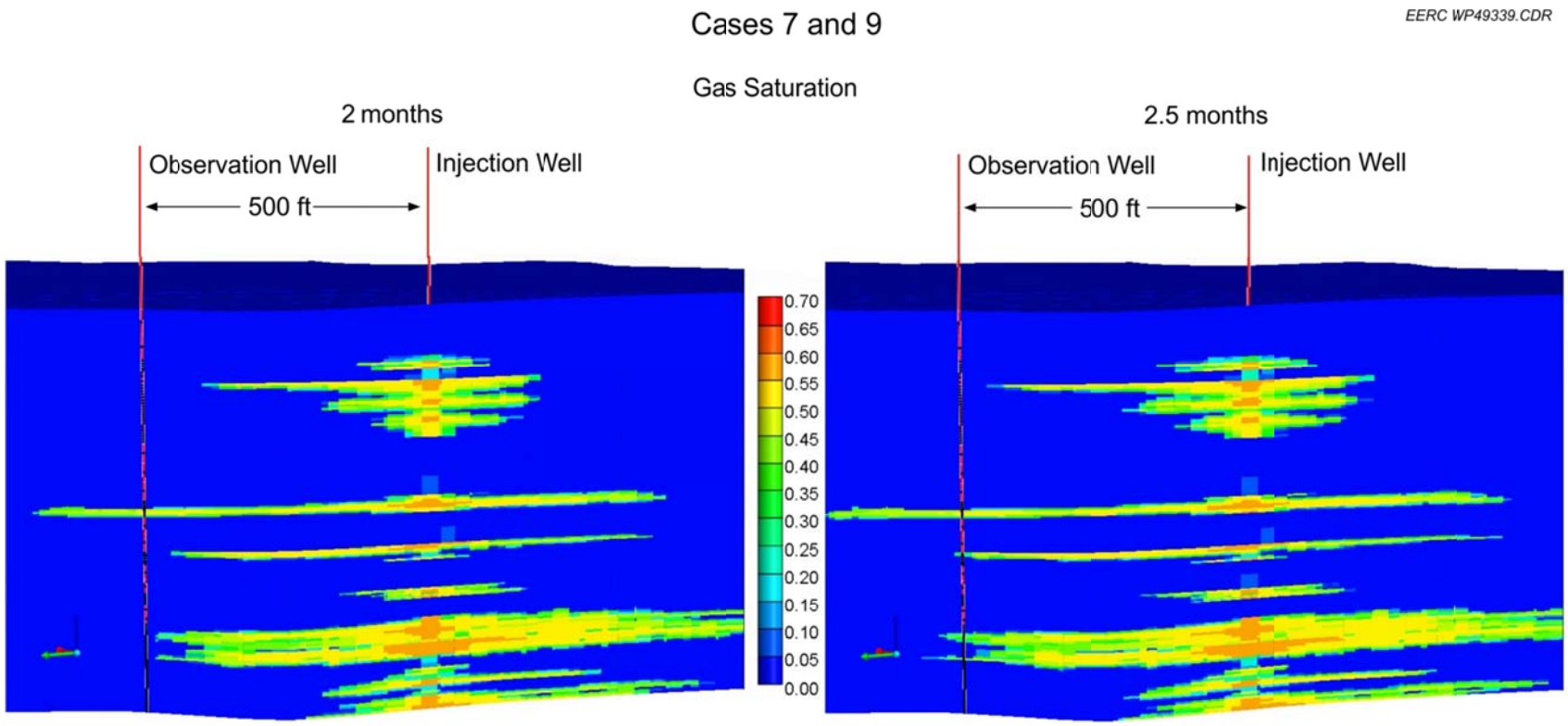

Figure A-9. Cross-sectional view of CO_2 breakthrough at the observation well in Cases 7 and 9 with low injection rate, 0.3 Mt/year utilizing the relative permeability tested by the Energy & Environmental Research Center (EERC) Applied Geology Laboratory. After 3 months of injection, the CO_2 breakthrough happened in most reservoir zones.

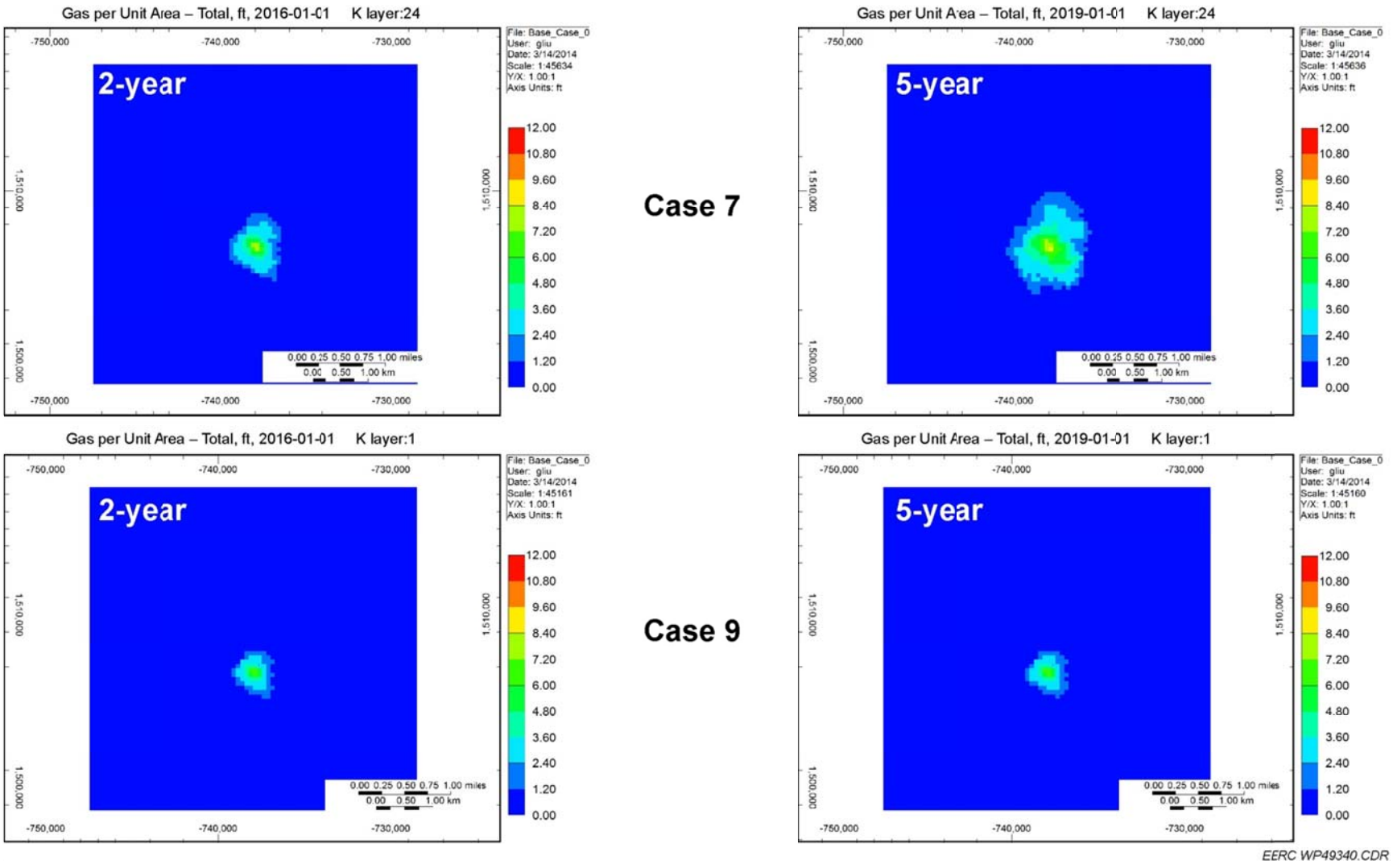

Figure A-10. Plane view of CO_2 plume with low injection rate, 0.3 Mt/year in Cases 7 and 9 for utilizing the relative permeability tested by the EERC Applied Geology Laboratory after 2 years and 5 years.